NASA TECHNICAL MEMORANDUM

NASA TM X-3332

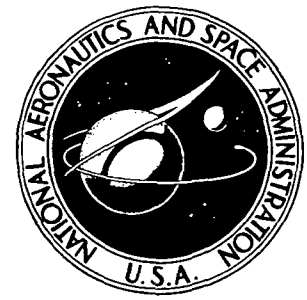


NASA TM X-3332



# LOW-SPEED WIND-TUNNEL INVESTIGATION OF THE AERODYNAMIC AND ACOUSTIC PERFORMANCE OF SEVERAL SONIC INLET TAKEOFF AND APPROACH GEOMETRIES

*John M. Abbott and Richard L. Golladay*

*Lewis Research Center*
*Cleveland, Ohio 44135*


NATIONAL AERONAUTICS AND SPACE ADMINISTRATION • WASHINGTON, D. C. • FEBRUARY 1976

| 1. Report No. | 2. Government Accession No. | 3. Recipient's Catalog No. |
|---|---|---|
| NASA TM X-3332 | | |

| 4. Title and Subtitle | 5. Report Date |
|---|---|
| LOW-SPEED WIND-TUNNEL INVESTIGATION OF THE AERODYNAMIC AND ACOUSTIC PERFORMANCE OF SEVERAL SONIC INLET TAKEOFF AND APPROACH GEOMETRIES | February 1976 |
| | 6. Performing Organization Code |

| 7. Author(s) | 8. Performing Organization Report No. |
|---|---|
| John M. Abbott and Richard L. Golladay | E-8445 |
| | 10. Work Unit No. 505-05 |

| 9. Performing Organization Name and Address | 11. Contract or Grant No. |
|---|---|
| Lewis Research Center<br>National Aeronautics and Space Administration<br>Cleveland, Ohio 44135 | |

| 12. Sponsoring Agency Name and Address | 13. Type of Report and Period Covered |
|---|---|
| National Aeronautics and Space Administration<br>Washington, D.C. 20546 | Technical Memorandum |
| | 14. Sponsoring Agency Code |

15. Supplementary Notes

16. Abstract

A series of tests was conducted to determine the aerodynamic and acoustic performance of several sonic inlet takeoff and approach geometries. The effects of inlet lip shape and diffuser length were also investigated. The tests were conducted in a low-speed wind tunnel at free-stream velocities of 0 and 45 meters per second. Inlet incidence angle was varied from $0^{o}$ to $50^{o}$. The inlets were sized to fit a 13.97-centimeter-diameter fan. In terms of the highest level of inlet total pressure recovery for a given amount of noise suppression, a cylindrical centerbody takeoff geometry and a bulb-shaped centerbody approach geometry provided the best results over all conditions of free-stream velocity and incidence angle. Increasing inlet lip contraction ratio extended the maximum incidence angle for attached lip flow, while increasing inlet diffuser length resulted in a higher total pressure recovery for a given amount of noise suppression.

| 17. Key Words (Suggested by Author(s)) | | 18. Distribution Statement |
|---|---|---|
| Sonic inlet | Wind tunnel tests | Unclassified - unlimited |
| Choked inlet | Acoustic suppression | STAR Category 07 (rev.) |
| Inlet design | | |

| 19. Security Classif. (of this report) | 20. Security Classif. (of this page) | 21. No. of Pages | 22. Price* |
|---|---|---|---|
| Unclassified | Unclassified | 48 | $3.75 |

* For sale by the National Technical Information Service, Springfield, Virginia 22161

# LOW-SPEED WIND-TUNNEL INVESTIGATION OF THE AERODYNAMIC AND ACOUSTIC PERFORMANCE OF SEVERAL SONIC INLET TAKEOFF AND APPROACH GEOMETRIES

by John M. Abbott and Richard L. Golladay

Lewis Research Center

## SUMMARY

A series of tests were conducted to determine the aerodynamic and acoustic performance of several sonic inlet takeoff and approach geometries. Two takeoff geometries were tested; they were (1) the cylindrical centerbody and (2) the bulb-shaped centerbody. Five approach geometries were tested; they were the following: (1) bulb-shaped centerbody, (2) centerbody-annular ring, (3) annular ring, (4) radial vane, and (5) step diffuser. The effects of inlet lip shape and diffuser length were also investigated.

The tests were conducted in a low-speed wind tunnel at free-stream velocities of 0 and 45 meters per second. Inlet incidence angle was varied from $0^{\circ}$ to $50^{\circ}$. The inlets were sized to fit a 13.97-centimeter-diameter fan.

In terms of the best inlet total pressure recovery for a given amount of noise suppression, the cylindrical centerbody takeoff geometry and the bulb-shaped centerbody approach geometry provided the best results over all conditions of free-stream velocity and incidence angle. With 20 decibels of noise suppression, the cylindrical centerbody takeoff geometry had a total pressure recovery of 0.988 at a free-stream velocity of 45 meters per second and an incidence angle of $0^{\circ}$. At the same free-stream velocity and incidence angle, the bulb-shaped centerbody approach geometry provided 15 decibels of suppression with a recovery of 0.968.

Increasing inlet lower lip area contraction ratio from 1.30 to 1.44 increased the maximum incidence angle for attached lip flow from $40^{\circ}$ to at least $50^{\circ}$ for the cylindrical centerbody takeoff geometry at a free-stream velocity of 45 meters per second. In general, increasing inlet diffuser length resulted in an increase in noise suppression at a given value of total pressure recovery.

## INTRODUCTION

It has been shown that aircraft engine noise radiated forward through the inlet can be reduced by accelerating the engine airflow to sonic or near sonic velocity in the inlet throat (refs. 1 to 7). Engine noise reduction is desirable whenever the aircraft is near the ground, that is, at both takeoff and approach. If the engine airflow at approach is much less than at takeoff, it may be necessary to provide a means of varying the inlet throat area to maintain sonic throat velocity at both conditions. This variation in geometry can be accomplished in many ways including the translation of variously shaped centerbodies, annular rings and vanes, and the expansion of centerbodies and cowl walls.

An investigation was undertaken at the Lewis Research Center to evaluate the aerodynamic and acoustic performance of several of these takeoff and approach sonic inlet geometries at scale model size in a low-speed wind tunnel. Two takeoff geometries were tested: (1) cylindrical centerbody; and (2) bulb-shaped centerbody. Five approach geometries were tested: (1) bulb-shaped centerbody; (2) centerbody-annular ring; (3) annular ring; (4) radial vanes; and (5) step diffuser. One of these inlet geometries (the cylindrical centerbody takeoff geometry) had been tested previously in a low-speed wind tunnel (ref. 2).

In evaluating these different geometries, both aerodynamic and acoustic performance are considered. At takeoff, where full engine thrust is required, the inlet geometry should provide the desired level of acoustic suppression with a high level of total pressure recovery and a level of total pressure distortion acceptable to the engine fan. At approach, the acoustic suppression should be obtained with a level of distortion acceptable to the fan, but, a high level of total pressure recovery is not as important because of the reduced level of engine thrust required during approach.

In addition to evaluating these different techniques for providing a variation in throat area, the effects of inlet internal lip shape and diffuser length on sonic inlet performance were also investigated. Inlet lip shape may be a particularly important consideration for sonic inlets intended for powered-lift short-haul aircraft applications. For this type of aircraft, high local flow angles can be encountered on the inlet lower lip as a consequence of the high upwash flow field generated by the powered-lift engine-wing system (ref. 8). It is important that the airflow remain attached to the inlet lip with these high incidence angles in order to avoid any reduction in total pressure recovery or increase in total pressure distortion due to lip flow separation.

Inlet diffuser length is an important consideration because the desire to keep the inlet as short as possible is in conflict with the high inlet flow Mach number changes necessarily involved with sonic inlets. This is most evident at approach where the engine airflow (and fan face Mach number) is lowest and yet the throat Mach number must be high in order to obtain the acoustic suppression. The throat-to-fan face Mach number

change is not as severe at takeoff because of the higher inlet weight flow. However, it is still greater than that for a conventional inlet where the throat Mach number is considerably lower.

The inlets were designed to fit a 13.97-centimeter-diameter fan and provided choked flow at takeoff and approach weight flows typical for proposed short-haul powered-lift aircraft; 100 percent and 78 percent of fan design weight flow. The relatively high approach weight flow is a consequence of the engine being used to supply both thrust and lift during the aircraft approach.

The inlets were tested at free-stream velocities of 0 and 45 meters per second and incidence angles from $0^{\circ}$ to $50^{\circ}$. These values represent the range of flight conditions expected for short-haul powered-lift aircraft during takeoff and approach.

Data presented include inlet total pressure recovery, total pressure distortion, total pressure distribution, surface static pressure distribution, and acoustic suppression. Results for the takeoff and approach geometries are presented first, and then the effects of inlet lip and diffuser design are examined.

## SYMBOLS

| | |
|---|---|
| $A_{DE}$ | diffuser exit flow area |
| $A_{TH}$ | throat area |
| a | ellipse semi-major axis of internal lip |
| BPF | blade passing frequency |
| b | ellipse semi-minor axis of internal lip |
| $D_{DE}$ | diffuser exit diameter |
| $D_{max}$ | inlet total pressure distortion parameter, eq. (1) |
| $L_D$ | diffuser length |
| $L_1$ | cowl length |
| $L_2$ | bulb-shaped centerbody length |
| $M_{TH}$ | one-dimensional average throat Mach number |
| $P_1$ | total pressure at diffuser exit |
| $P_{1,av}$ | area averaged total pressure at diffuser exit |
| $(P_{1,av})_c$ | circumferentially averaged diffuser exit total pressure at constant radius |
| $P_0$ | free-stream total pressure |

| | |
|---|---|
| $p_s$ | surface static pressure |
| r | radius |
| $r_{HL}$ | radius at highlight |
| $r_{max}$ | maximum cowl radius |
| $r_{TH}$ | radius at throat |
| $V_0$ | free-stream velocity |
| $\% \dot{w}_D$ | percent design corrected weight flow |
| $X_1$ | axial distance from cowl highlight |
| $X_2$ | axial distance from bulb-shaped centerbody leading edge |
| $\alpha$ | incidence angle, deg |
| $(\Delta SPL)_{BPF}$ | one-third-octave band sound pressure level reduction at blade passing frequency (fig. 6) |
| $\lambda_{max}$ | maximum diffuser wall angle, deg |
| $\psi$ | inlet circumferential position, deg |

## APPARATUS

### Installation

Shown in figure 1 is a general layout of the test installation in the Lewis Research Center's 9- by 15-Foot V/STOL Wind Tunnel (ref. 9). The model was mounted on a turntable for testing over a range of incidence angles. Microphones were located upstream of the test section in a low flow velocity reverberant area of the wind tunnel to measure inlet radiated noise.

The test model consisted of test inlets, a fan, exhaust ducting, and an exhaust noise muffler. The single stage, 13.97-centimeter-diameter, tip turbine driven fan was used both as a suction source and noise generator. The fan has 16 rotor blades resulting in a blade passing frequency of 9600 hertz at the fan design speed of 36 000 rpm. Design pressure ratio is 1.25 at a weight flow of 2.49 kilograms per second. More details of fan performance are given in reference 10. The fan exhaust was ducted out of the test section and into a noise muffler to permit an examination of only the noise being radiated forward through the inlet.

## Inlet Design

The inlets discussed in this report were designed to provide the necessary throat area reduction to choke at 100 and 78 percent of fan design weight flow (2.49 kg/sec), values estimated to be typical for short-haul powered-lift aircraft designs during takeoff and approach. The corresponding diffuser area ratios $A_{DE}/A_{TH}$ for takeoff and approach are 1.30 and 1.65, respectively. The sonic inlet takeoff and approach geometries tested are shown in figure 2 along with a baseline geometry with a short spinner (normal cruise configuration).

The inlet geometries could be considered as belonging to two distinct groups depending on the number of throat flow passages. The radial vanes and annular rings result in multiple-passage geometries as opposed to the other single-passage geometries. The multiple-passage geometries are of interest because, for a given rate of flow diffusion (change in flow area per unit length in one passage), the same overall area increase can be accomplished in a shorter distance with a number of individual flow passages as opposed to a single flow passage. For a sonic inlet, where the airflow must be diffused from a throat Mach number of 1.0 to a fan face Mach number of 0.5 (or possible lower) at approach, this can result in a significant reduction in diffuser and overall inlet length.

Important dimensions for inlet components used to provide the sonic inlet throat area variations are shown in figure 3.

Some of the inlet geometries were tested with different cowl designs to determine the effects of lip and diffuser design on aerodynamic and acoustic performance. There were a total of four different cowl designs designated by the letters A, B, C, and D. (Cowl B was tested previously with the cylindrical centerbody takeoff geometry as reported in ref. 2.) Important design parameters are given in figure 4. Briefly, two lip designs were tested with lower lip contraction ratios $(r_{HL}/r_{TH})^2$ of 1.30 and 1.44. The 1.30 contraction ratio cowls (A and B) have symmetric lips with an elliptical internal lip shape having a semi-major to semi-minor axis ratio a/b of 2.0. The external lip shape is an NACA series 1 contour with a drag divergence Mach number of 0.80. The 1.44 contraction ratio cowls (C and D) are asymmetric having a contraction ratio of 1.44 only at the lower lip ($\psi = 0^{\circ}$) with a smooth circumferential transition to a value of 1.30 at the sides ($\psi = 90^{\circ}$) which is then maintained over the entire upper half of the lip. The internal lip ellipse ratio is 2.0 at the lower lip and transitions to a value of 2.9 at the sides which is also maintained over the entire upper half of the lip. The external lip contour is an ellipse with an a/b of 4.5. When referring to cowl C and D, the contraction ratio will be given as 1.44/1.30 and the internal lip ellipse ratio as 2.0/2.9.

Three different diffuser designs were tested having length-to-diameter ratios $L_D/D_{DE}$ of 0.43 (cowl A), 0.61 (cowls B and C), and 0.92 (cowl D). In all four cases,

the nondimensional diffuser contours were the same (ref. 1). Hence, by comparing data for cowls B and C, the effect of inlet lip design can be determined with the same diffuser design. By comparing data for cowls A and B and then cowls C and D, the effect of inlet diffuser length can be determined with the same lip design.

## Instrumentation and Data Reduction

Inlet aerodynamic instrumentation consisted of diffuser exit total pressure rakes (eight legs with six probes per leg each located at the centroid of equal flow areas) and surface static pressure taps on the cowls and bulb-shaped centerbody (fig. 5). These pressure measurements were used to calculate inlet total pressure recovery, total pressure distortion, inlet weight flow, and surface static- to total-pressure ratios.

The total pressure distortion parameter presented is defined as

$$D_{max} = \left( \frac{P_{1,max} - P_{1,min}}{P_{1,av}} \right)_{40} \tag{1}$$

Of the 48 total pressure measurements made at the diffuser exit, the eight total pressure measurements closest to the outer wall of the flow passage (0.26 cm from the outer wall and in the boundary layer) were not included in the calculation. The maximum and minimum values are $P_{1,max}$ and $P_{1,min}$, and $P_{1,av}$ is the area average of the remaining 40 total pressure measurements.

The inlet weight flow was computed from the 48 total and 7 static pressure measurements made at the diffuser exit. For this calculation, a calibration test was performed using a standard bellmouth inlet to determine the correction factor to be applied to the computed diffuser exit weight flow (a correction of about 3 percent). Inlet throat Mach number was computed from the calculated inlet weight flow and the inlet geometric throat area. It is presented only to a limited extent in this report because of its sensitivity to small errors in measured weight flow in the region of throat Mach number from 0.70 to 1.00 (e.g., a 1 percent error in weight flow reduces the calculated throat Mach number from 1.0 to 0.89).

Noise data were taken with 0.64-centimeter-diameter microphones located in the low velocity section of the wind tunnel upstream of the test section (fig. 1). Wind screens were placed on the microphones to minimize tunnel airflow noise. The hardwalls of the wind tunnel approximate a reverberant chamber eliminating any directional noise variation due to changing model incidence angle within the range of interest. The noise data were processed using a one-third-octave band analyzer (4-sec sample time).

Values of noise suppression in the one-third-octave band containing fan blade passing frequency were computed by subtracting the sound pressure level for the particular sonic inlet geometry (figs. 2(a) and (b)) from the corresponding level obtained with the baseline geometry with the same inlet cowl (fig. 2(c)). This subtraction was done at the same fan speed, free-stream velocity, and incidence angle for the sonic inlet and the baseline geometries.

The procedure is illustrated in figure 6, where one-third-octave band sound pressure level at the blade passing frequency is plotted against fan speed for the baseline geometry and a sample sonic inlet geometry at static conditions and at a free-stream velocity of 45 meters per second with an inlet incidence angle of $0^{\circ}$. The figure indicates that, at static conditions, the sonic inlet provides noise suppression nearly to the limiting static background level of about 49 decibels. With free-stream velocity it is expected that the inlet would continue to provide noise suppression down to this level. However, the operating tunnel background noise level is higher than the static background noise level and masks any reduction in noise level below about 60 decibels. The fact that the amount of inlet noise suppression for the sonic inlet geometry does not quite reach the background noise limits is a consequence of noise being radiated from other sources at the model other than the inlet, such as the model support structure and the rear noise muffler.

In the presentation of all the acoustic suppression data, the maximum amount of measurable noise suppression will be indicated. It should be remembered that, if an inlet geometry shows this amount of suppression, it may be actually providing much more suppression, and there may also be variations in suppression below this level that cannot be observed.

### Test Procedure

The test procedure consisted of setting free-stream velocity, setting inlet diffuser exit static pressure (weight flow), and varying inlet incidence angle. The diffuser exit static pressure was then changed (by changing fan speed) and the variation in incidence angle was repeated. Aerodynamic data were taken at incidence angles of $0^{\circ}$, $20^{\circ}$, $40^{\circ}$, and $50^{\circ}$. Acoustic data were taken only at inlet incidence angles of $0^{\circ}$, $20^{\circ}$, and $40^{\circ}$.

## RESULTS AND DISCUSSION

### Performance of Takeoff Geometries

During takeoff, where maximum thrust is required, it is desirable to have a high value of total pressure recovery and a value of total pressure distortion acceptable to

the fan. For this reason, in comparing the two takeoff geometries, the highest total pressure recovery and lowest total pressure distortion for a given amount of noise suppression is used as an aeroacoustic figure of merit.

Comparison of geometries. - In figure 7, inlet total pressure recovery and total pressure distortion for the two takeoff geometries with cowl B are shown as a function of inlet noise suppression at the fan blade passing frequency. Data are presented at static conditions (fig. 7(a)) and at a free-stream velocity of 45 meters per second with incidence angles of $0^{\circ}$ and $40^{\circ}$ (figs. 7(b) and (c), respectively). Selected values of inlet weight flow and throat Mach number are noted in the figure.

If the highest total pressure recovery for a given amount of noise suppression is used as an aeroacoustic figure of merit, the data of figure 7 indicate that, for all conditions of free-stream velocity and incidence angle, the cylindrical centerbody provides a higher level of performance than the bulb-shaped centerbody takeoff geometry. The negative values of noise suppression that appear in figure 7 may be due to either an increase in fan noise generation during operation with the sonic inlet or scatter in the noise data. Both inlet geometries are choking at a weight flow slightly less than the design value ($\simeq 97\%\ \dot{w}_D$) due to a nonuniform velocity profile in the inlet throat and a reduction in the throat flow area as a result of surface boundary layer growth. The increase in distortion and decrease in recovery encountered beyond the initial choke point in figure 7(a) is a consequence of supercritical operation of the inlet (solid symbols). In this region, shocks and boundary layer-shock interactions occur locally in the vicinity of the throat which result in the increase in total pressure losses. A more detailed discussion of each of the two takeoff geometries will be presented in the following sections.

Cylindrical centerbody takeoff geometry (cowl B). - This is the same inlet geometry that was reported on in detail in reference 2. Because of some minor changes in the model test installation, the inlet geometry was tested again and those data are presented here.

Statically (fig. 7(a)) the cylindrical centerbody takeoff geometry provided a maximum measurable noise suppression of about 33 decibels at the blade passing frequency with a total pressure recovery of 0.98 and a total pressure distortion of 0.02. The noise spectrum for this data point is shown in figure 8 and indicates that maximum suppression occurred over the frequency range from 3000 to 20 000 hertz. The higher noise levels at the lower frequencies are probably a result of noise radiation from the model support structure and the muffled rear noise becoming dominant.

Comparison of figures 7(a) and (b) indicates that there is no significant change in inlet performance as a result of introducing free-stream velocity. As discussed previously, the maximum amount of noise suppression measurable is lower in figure 7(b) due to the higher wind tunnel background noise level.

Increasing incidence angle to $40^{\circ}$ (fig. 7(c)) results in a slight decrease in total pressure recovery at values of noise suppression less than about 8 decibels. However,

for higher levels of noise suppression, the pressure recovery decreases at a faster rate and the total pressure distortion increases accordingly. The reason for this accelerated increase in total pressure losses is illustrated by the axial internal cowl surface static pressure distributions on the windward side ($\psi = 0^{\circ}$) shown in figure 9. At lower values of inlet noise suppression (% $\dot{w}_D \simeq 88$) (fig. 9(a)), increasing incidence angle results in a decrease in lower lip surface static pressure (increase in surface Mach number) until an incidence angle of $50^{\circ}$ where the flow separates from the inlet highlight as evident from the relatively flat surface static pressure distribution over the entire length of the inlet. At $40^{\circ}$ incidence angle, the flow is attached to the entire cowl surface and total pressure recovery at this point is 0.993. At the higher values of inlet noise suppression (% $\dot{w}_D \simeq 97$), the data of figure 9(b) indicate that at $40^{\circ}$ incidence angle, the inlet flow has separated from the diffuser wall and there is also an indication of a separation bubble (a small region of flow separation followed by reattachment) occurring on the lip. This is evident from the increase and then the decrease in surface static pressure between x/L values of 0.05 and 0.17. These separation phenomena at high values of inlet weight flow are what account for the drop in pressure recovery and increase in distortion encountered at an incidence angle of $40^{\circ}$ in figure 7(c). Note that at $50^{\circ}$ incidence angle the inlet diffuser remains separated in figure 9(b); however, the flow appears to be completely attached to the inlet lip.

The change in the distribution of total pressure at the diffuser exit as incidence angle is increased is described in detail in reference 2. Briefly, increasing incidence angle resulted in a significant decrease in the value of minimum total pressure in the lower half (or windward) portion of the inlet near the outer wall at the diffuser exit, even though the recovery decreased only slightly. The net effect then was an increase in total pressure distortion, particularly circumferential distortion, with increasing incidence angle.

Bulb-shaped centerbody takeoff geometry (cowl B). - As indicated in figure 7(a), at static conditions this takeoff geometry provided a maximum of 30 decibels of noise suppression at the blade passing frequency with a total pressure recovery of 0.962 and a total pressure distortion of 0.17. Over much of the noise suppression range at static conditions, this geometry provided a total pressure recovery that was about 0.6 percent less than the cylindrical centerbody geometry. A more detailed examination of the data indicated that the increase in losses was occurring near the outer wall at the diffuser exit. This is believed to be a result of an increase in cowl lip surface velocities (as confirmed by the surface static pressure measurements) induced by the presence of the forward extended bulb-shaped centerbody. Statically, the suppressed acoustic spectrum was nearly identical to that shown for the cylindrical centerbody geometry (fig. 8).

By comparing figures 7(a) and (b), it can be seen that the aeroacoustic performance of this inlet geometry is not as good with free-stream velocity as it was statically. In

fact, in figure 7(b), the maximum amount of measurable suppression was not obtained.

Increasing incidence angle to $40^{\circ}$ results in a further decrease in aeroacoustic performance (lower recovery, higher distortion) as shown in figure 7(c). An examination of the cowl surface static pressure distributions indicated that at $40^{\circ}$ incidence angle, a separation bubble had apparently formed on the inlet lip and in some cases the inlet flow was separating from the diffuser wall. At $50^{\circ}$ incidence angle, the flow was separated at the inlet highlight.

Surface static pressure profiles for the centerbody are shown in figure 10. Even at the highest values of inlet weight flow, no surface flow separation was apparent on the extended bulb-shaped centerbody up to an incidence angle of $40^{\circ}$. At $50^{\circ}$ incidence angle, a reversal in the trend of decreasing static pressure with increasing incidence angle is apparent at the $\psi = 0^{\circ}$ position (fig. 10(a)). However, an examination of the total pressure distribution at the diffuser exit did not indicate the presence of a flow separation from the centerbody.

The distribution of total pressure at the inlet diffuser exit is shown in figure 11 at incidence angles of $0^{\circ}$, $20^{\circ}$, $40^{\circ}$, and $50^{\circ}$ for the maximum value of inlet weight flow. At $0^{\circ}$ incidence angle (fig. 11(a)) the total pressure distribution is axisymmetric with the total pressure losses occurring at both the inner and outer wall due to supercritical operation. Figure 11(b) indicates that, at $20^{\circ}$ incidence angle, the total pressure losses are beginning to concentrate at the $\psi = 0^{\circ}$ position at both the outer and inner wall. At $40^{\circ}$ incidence angle, where lip and diffuser separations were encountered, the inlet total pressure losses are now concentrated at the outer wall only (fig. 11(c)). The local total pressure recovery is very high around the entire circumference at the inner wall. Inlet lip separation at the highlight occurred at an incidence angle of $50^{\circ}$ (fig. 11(d)) resulting in the extended region of low total pressure in the windward portion at the diffuser exit.

## Performance of Approach Geometries

The problem of deciding which geometry provides the best aeroacoustic performance is more difficult for the approach geometries than for the takeoff geometries. As noted previously, at takeoff where full engine thrust is required, it is desirable to have a high level of inlet total pressure recovery. However, at approach the engine is not operating at full thrust and a high value of total pressure recovery may not be as important. The required approach thrust level can be obtained with a lower inlet pressure recovery by operating the engine at a higher rotational speed. Hence, in evaluating the inlet approach geometries, it should be remembered that the inlet recovery may not be the most important consideration and that other aerodynamic performance indicators such as diffuser exit total pressure distribution and the character of the total pressure distortion

(circumferential or radial) may be of more importance.

Comparison of geometries. - Figure 12 presents the aerodynamic and acoustic performance of the five approach geometries. The data are presented in the same format as figure 7 for the takeoff geometries. Inlet weight flow and throat Mach number are indicated in the figure only for the two single passage geometries. Values are not given for the multipassage geometries because of the inaccuracy in the calculation resulting from the vane, ring, and strut wakes and the losses generated in the corners where the struts intersect the rings and centerbodies.

In figure 12 the inlet cowl is not the same for each approach geometry. For various reasons, it was not possible to present test results with all the geometries having the same cowl. However, the relative performance of each of the geometries is felt to be well represented by the data of figure 12. A discussion of cowl design effects will be presented in subsequent sections on the effects of lip and diffuser design.

Figure 12 indicates that at all conditions of free-stream velocity and incidence angle, the single-passage bulb-shaped centerbody approach geometry provided the highest pressure recovery at a given level of noise suppression. Statically (fig. 12(a)) the bulb-shaped centerbody geometry had the lowest total pressure distortion. However, with a free-stream velocity of 45 meters per second and an incidence angle of $40^{\circ}$ (fig. 12(c)) the total pressure distortion of this geometry increased to the point where it was slightly greater than the three multipassage geometries. Detailed results for each of the five approach geometries will be presented in the following sections.

Bulb-shaped centerbody approach geometry (cowl B). - At static conditions (fig. 12(a)) this approach geometry provided a maximum noise suppression of 33 decibels at the blade passing frequency with a total pressure recovery of 0.973 and a total pressure distortion of 0.16. For a given amount of suppression, the values of recovery are about the same as they were for the bulb-shaped centerbody takeoff geometry (fig. 7(a)). The distortions are higher, however, due to a slight increase in the extent of the total pressure losses in the outer wall region at the diffuser exit. The result of supercritical operation beyond the initial choke point is again evident by the drop in total pressure recovery and, in this case, a substantial drop in noise suppression.

A frequency spectrum for the maximum noise suppression data point at static conditions is shown in figure 13. Again, noise suppression occurred over the entire frequency range. At frequencies below 1000 hertz, the bulb-shaped centerbody approach geometry indicates a greater amount of noise suppression than the cylindrical centerbody takeoff geometry (fig. 8). This may be a result of differences in muffled rear noise levels which become dominant as the inlet radiated noise is suppressed. At approach, where the weight flow is reduced, the rear noise levels would be expected to be lower.

The performance at a free-stream velocity of 45 meters per second and an incidence angle of $0^{\circ}$ is shown in figure 12(b). At the lower values of inlet noise suppres-

sion (less than about 7 dB), the total pressure recovery is about the same as it was at static conditions. At the highest level of inlet noise suppression, the data of figure 12(b) indicate that the total pressure recovery is lower than it was statically.

Increasing incidence angle from $0^{\circ}$ to $40^{\circ}$ (fig. 12(c)) resulted in about a 1 percent decrease in inlet pressure recovery and increase in distortion at a given level of noise suppression. This increase in total pressure losses is a result of a larger amount of required diffusion (corresponding to lower static pressure, fig. 14(a)) on the windward portion of the inlet lip at an incidence angle of $40^{\circ}$. Shock-boundary layer interactions might also contribute to the losses.

At $50^{\circ}$ incidence angle, the static pressure distribution in figure 14(a) indicates that flow separation was encountered on the inlet lip downstream of the highlight. Figure 14(b) indicates that there is also a possible local flow separation on the windward side of the bulb-shaped centerbody at an incidence angle of $50^{\circ}$. This is believed to be indicated by the change in slope of the surface static pressure distribution at an $x_2/L_2$ position of about 0.65.

Although data are not shown, the radial and circumferential distribution of total pressure at the diffuser exit was very similar to that encountered with the bulb-shaped centerbody takeoff geometry. At high inlet weight flows, the total pressure distribution was axisymmetric at $0^{\circ}$ incidence angle but the regions of lower total pressure tended to move toward the windward portion of the inlet duct as incidence angle was increased.

Centerbody-annular ring approach geometry (cowl B). - As shown in figure 12(a), large reductions in blade passing frequency noise levels were obtained with this geometry at static conditions with the total pressure recovery ranging from a maximum value of 0.977 to a minimum of 0.934. However, a closer look at the entire noise spectra indicated that the suppression shown in figure 12(a) was not occurring across the entire frequency range. Presented in figure 15 is the noise spectrum at the condition of maximum blade passing frequency suppression. As can be seen, at some of the lower frequencies, the inlet geometry was actually producing more noise than the baseline geometry shown in the figure. There are a number of possible sources for this acoustic behavior including vibration of the ring itself. It seems more likely, however, that increased fan noise generation due to the annular ring and support strut wakes may be somehow propagating forward through the inlet.

The higher total pressure losses encountered with this geometry are due to the annular ring and support strut wakes and losses generated in the corners where the struts intersect the ring and centerbody. An additional source of losses as the inlet weight flow increased was a mismatch in geometric flow areas between the inner and outer annular flow passages. The annular ring was located within the inlet flow duct such that the ring airfoil chord line passed through the centroid of the local flow area at two points; the cowl throat plane and the axial location of the ring airfoil trailing edge. This resulted in the ring airfoil chord line not being parallel to the inlet centerline as indicated

in figure 3(d). This ring alinement in combination with the airfoil thickness resulted in unequal geometric throat areas between the inner and outer flow passages. In fact, the inner passage minimum geometric flow area was smaller than the outer and occurred upstream of the cowl throat plane. As a result of this throat area mismatch, in order to choke the outer flow passage, the inner flow passage would necessarily be operating supercritically. This, of course, creates an additional source of inlet total pressure losses.

At a free-stream velocity of 45 meters per second and an incidence angle of $0^{\circ}$ there was little change in performance as shown in figure 12(b). An examination of the entire spectrum at the maximum blade passing frequency suppression level for this condition (not shown), indicates complete suppression down to the wind tunnel background level at all frequencies. However, the lower frequency noise, which was not suppressed at static conditions, is now below the wind tunnel noise background level and it cannot be determined whether or not it is still present.

Increasing incidence angle to $40^{\circ}$ (fig. 12(c)) resulted in an increase in inlet total pressure losses as a result of flow separations encountered on the windward portion of the internal cowl surface. It is also possible that flow separation was occurring on the annular ring, however, without static pressure measurements on the ring surfaces this could not be confirmed. Also, the total pressure distortion has increased slightly.

Annular ring approach geometry (cowl D). - With this inlet geometry at static conditions (fig. 12(a)) low total pressure recoveries and high distortions were encountered due to the annular ring and support strut wakes, corner losses and because of the same flow passage area mismatch problem just discussed for the centerbody-annular ring geometry. In addition to this, figure 12(a) indicates that the suppression levels obtained with the annular ring geometry were much lower than any of the other geometries. The spectrum at the maximum blade passing frequency suppression data point is shown in figure 16. In this case, over a large percentage of the frequency range, this inlet geometry has higher noise levels than the baseline geometry shown in the figure. As discussed before, possible sources for these noise levels are transmission via the annular ring or ring vibration and increased fan noise due to the ring and strut wakes. Free-stream velocity and incidence angle (figs. 12(b) and (c)) have about the same effect on the aerodynamic performance with this geometry as the centerbody-annular ring geometry. However, with this geometry, the high noise levels shown statically in figure 16 can also be seen above the tunnel background level.

Radial vane approach geometry (cowl C). - At static conditions (fig. 12(a)) this geometry provided a maximum of 29.5 decibels of suppression at the blade passing frequency with a total pressure recovery of 0.905 and a total pressure distortion of 0.17. Again, the vane wakes and corner losses contribute to this low recovery and high distortion. The frequency spectrum at the maximum suppression point (fig. 17) indicates that

the suppression is occurring across the frequency range although the levels are not quite down to the background level.

As indicated in figure 12(a), the inlet total pressure recovery takes a rather rapid drop from a value of 0.975 to 0.930 at a suppression level of around 7 decibels. This rapid increase in total pressure losses is attributed to passing through the drag rise region for this particular airfoil section (NACA $63_2$A015). In this region, attempts to increase inlet airflow by increasing fan speed result in increases in inlet total pressure losses which tend to offset the effect of increased fan speed. After passing through this region, inlet weight flow again increases, and the high levels of acoustic suppression are finally approached as the inlet chokes. This result suggests that by designing this type of inlet with an airfoil section having a smaller thickness-to-chord ratio the performance should improve. With a finer airfoil section, a higher drag rise Mach number would result and a greater inlet weight flow, and hence a greater amount of acoustic suppression, could be obtained before the drag rise total pressure losses were encountered.

An examination of the total pressure radial distribution at the diffuser exit (fig. 18) suggests another source of inlet total pressure losses for the radial vane geometry. As the figure shows, as inlet weight flow is increased, the total pressure losses become much more dominant in the hub region. This can be explained by the fact that the solidity (ratio of vane chord length to vane spacing) is higher in the hub region than in the tip region because of the constant chord length of the vanes. This higher solidity then results in higher losses at the hub. A possible solution to this problem would be to taper the vanes such that they would have a shorter chord length (and lower solidity) in the hub region.

With free-stream velocity and incidence angle (figs. 12(b) and (c)), the total pressure recovery and distortion remained relatively unchanged. The sudden drop in recovery at a given level of suppression corresponding to the drag rise region remains in both figures.

Step diffuser approach geometry (cowl B). - As noted in the discussion of all the single-passage geometries, increasing incidence angle results in an increase in the extent of the total pressure losses in the lower portion of the diffuser exit. This in turn means that the circumferential total pressure distortion is changing and increasing with higher incidence angles. Such loss patterns may present a potential problem to the engine fan designer. The design philosophy adopted with the step diffuser approach geometry was to force the total pressure losses to occur at the tip around the entire circumference. Hopefully, with increasing incidence angle, the losses would remain circumferentially uniform, thus eliminating the changes in circumferential distortion at the expense of a constant, known radial distortion. It was recognized that the total pressure losses would be high.

As figure 12 indicates, the total pressure recovery for this geometry was the lowest of all those tested, but comparable inlet noise suppression was provided. The noise spectrum indicated suppression across the entire frequency range and free-stream velocity and incidence angle had practically no effect on aerodynamic and acoustic performance.

Shown in figure 19 are total pressure distributions at the diffuser exit at incidence angles of $0^{\circ}$ and $50^{\circ}$. The figure indicates that, as expected, the total pressure distribution did not change with increasing incidence angle. The circumferential variation in total pressure remained unchanged and essentially zero over the incidence angle range from $0^{\circ}$ to $50^{\circ}$.

## Effect of Cowl Lip Design

The effects of inlet lip design will be discussed for both the cylindrical centerbody takeoff geometry and the bulb-shaped centerbody approach geometry.

Cylindrical centerbody takeoff geometry. - In figure 20, aerodynamic results are presented for cowls B and C having lip contraction ratios of 1.30 and 1.44/1.30 and internal lip ellipse ratios of 2.0 and 2.0/2.9, respectively. Inlet total pressure recovery is plotted against percent design corrected weight flow at a free-stream velocity of 45 meters per second and incidence angles of $0^{\circ}$, $40^{\circ}$, and $50^{\circ}$.

It is apparent from comparing the total pressure recovery data of figures 20(a) and (b) that increasing inlet lower lip contraction ratio from 1.30 to 1.44 results in an increase in the maximum incidence angle obtainable before lip flow separation occurs. With the 1.30 contraction ratio inlet at an incidence angle of $40^{\circ}$ and at high values of inlet weight flow, the appearance of lip separation bubbles, as previously discussed, is evident from the slight drop in recovery. At $50^{\circ}$ incidence angle, the recovery data indicate complete flow separation from the inlet lower lip. With the 1.44 lower lip contraction ratio inlet (cowl C) the inlet lip flow remains completely attached up to an incidence angle of at least $50^{\circ}$. Flow separation on the lower lip was avoided with cowl C at $50^{\circ}$ incidence angle because of the lower surface Mach numbers and milder Mach number gradients resulting from an increase in lip area contraction ratio. This result is confirmed by the detailed theoretical analysis of the effects of inlet lip shape on aerodynamic performance given in reference 11.

The effect of inlet lip design on the acoustic performance of the cylindrical centerbody takeoff geometry is shown in figure 21. Data are shown with inlet cowls B and C at static conditions (fig. 21(a)) and at a free-stream velocity of 45 meters per second with incidence angles of $0^{\circ}$ and $40^{\circ}$ (figs. 21(b) and (c), respectively). Two major differences between the acoustic performance of the inlet with cowls B and C are apparent from the

figure. First, with cowl C (having an internal lip ellipse ratio of 2.0/2.9) the inlet does not provide the maximum amount of measurable noise suppression, while the inlet with cowl B (a/b = 2.0) does. This is particularly evident at static conditions where the inlet with cowl B provides 33 decibels of suppression while with cowl C, only 14 decibels. Spectra for these two data points (solid symbols in fig. 21(a)) are shown in figure 22 and indicate this loss in suppression capability with cowl C is occurring at all frequencies above about 5000 hertz. Spectra for the baseline geometry with cowls B and C are also shown in the figure. Secondly, figure 21 shows that at high values of pressure recovery (low values of weight flow), operation of this inlet geometry with cowl C results in an increase in fan noise generation (particularly evident in figs. 21(b) and (c)) and is actually generating up to 10 decibels more noise than the baseline geometry (negative values of suppression).

These differences in acoustic behavior observed with cowl C may be a result of a local flow separation occurring on the upper half to the inlet lip where the ellipse ratio is 2.9 ($\psi = -90^{\circ}$ to $+90^{\circ}$). If this lip flow separation does exist then the result could be a region of lower flow velocity in the inlet throat providing for a forward noise propagation path. This in turn could lead to the reduction in maximum measurable noise suppression indicated in figures 21 and 22. Also, a change in character of the fan inflow due to a local lip flow separation could lead to an increase in fan source noise. This could then account for the negative values of suppression in figure 21.

There is some indication in the lip surface static pressure data that a local flow separation bubble may indeed be occurring on the upper lip ($\psi = 180^{\circ}$, a/b = 2.9), although with the limited number of measurements it cannot be determined for certain that this is the case. However, there is an increased likelihood for local flow separation to occur with a larger ellipse ratio as discussed in reference 11. There it is shown that increasing internal lip ellipse ratio results in higher rates of surface curvature leading to higher surface velocities and unfavorable boundary layer conditions near the inlet highlight. This in turn may result in local lip flow separation.

In addition, the effects of inlet lip design (using 20.8-cm-diam inlets) were investigated in reference 7 with acoustic results very similar to those reported here. Sonic inlets having internal lip ellipse ratios of 2.0, 3.0, and 4.0 were tested. The data for the ellipse ratio of 2.0 showed complete acoustic suppression as did the results for cowl B (a/b = 2.0) in figure 21. However, the data for the ellipse ratios of 3.0 and 4.0 in reference 7 did not show complete acoustic suppression, with results nearly identical to those presented for cowl C (a/b = 2.9) in figures 21 and 22.

It should be mentioned that at full scale, because of scale effects on boundary layer development, the aerodynamic behavior described here may not occur, and the inlet acoustic performance with cowl C may improve accordingly.

Bulb-shaped centerbody approach geometry. - Figure 23 presents the aerodynamic performance of the two lip designs of cowls B and C with the bulb-shaped centerbody

approach geometry. The effect of lip design on aerodynamic performance is not as dramatic for this geometry as for the cylindrical centerbody takeoff geometry. This may be a consequence of the already lower surface Mach numbers resulting from operation at the lower approach weight flow. However, the higher lower-lip area contraction ratio of cowl C does result in a general improvement in aerodynamic performance as incidence angle is increased.

Aeroacoustic results are presented in figure 24 at static conditions (fig. 24(a)) and at a free-stream velocity of 45 meters per second at incidence angles of $0^{\circ}$ and $40^{\circ}$ (figs. 24(b) and (c), respectively). Statically, the results of supercritical operation with cowl B are indicated by the sudden loss of noise suppression and drop in recovery after the maximum value of noise suppression has been attained. With cowl C, there was again some indication in the lip surface static pressure data that a separation bubble may have existed on the upper lip at the $\psi = 180^{\circ}$ position (a/b = 2.9) at static conditions as was the case with the cylindrical centerbody takeoff geometry. The amount of noise suppression at the blade passing frequency is also limited, although in this case to a higher value of 25 decibels out of a measurable 40 decibels.

With a free-stream velocity of 45 meters per second, the amount of suppression obtained with cowl C at inlet incidence angles of $0^{\circ}$ and $40^{\circ}$ is closer to that obtained with cowl B (figs. 24(b) and (c)) than it was with the cylindrical centerbody takeoff geometry (fig. 21). Also, the increased fan noise generation (negative $(\Delta SPL)_{BPF}$) evident with the cylindrical centerbody takeoff geometry with cowl C is not present. Hence, the acoustic performance of the bulb-shaped centerbody approach geometry with cowl C is not adversely affected to the same degree as the cylindrical centerbody takeoff geometry. This again may be due to the reduced internal lip surface velocities encountered at the approach weight flow resulting in an overall improvement of the cowl lip performance.

In summary, increasing inlet lower lip contraction ratio from 1.30 (cowl B) to 1.44 (cowl C) resulted in an increase in the maximum inlet incidence angle for lip flow separation from $40^{\circ}$ to at least $50^{\circ}$ for the cylindrical centerbody takeoff geometry. However, the acoustic performance of this inlet geometry was adversely affected by the lip design of cowl C which had a lip ellipse ratio of 2.0/2.9. With the bulb-shaped centerbody approach geometry, cowl C also provided attached inlet lip flow up to an inlet incidence angle of at least $50^{\circ}$. The acoustic performance of this geometry at static conditions was again adversely affected by the lip design of cowl C. However, with free-stream velocity at incidence angles of $0^{\circ}$ and $40^{\circ}$, the suppression was comparable to that of cowl B.

## Effect of Cowl Diffuser Design

The effects of inlet diffuser length will be discussed for both the cylindrical center-

body takeoff geometry and the bulb-shaped centerbody approach geometry.

Cylindrical centerbody takeoff geometry. - In figure 25, the aerodynamic performance of cowls A and B are compared having the same inlet lip shape (contraction ratio of 1.30, ellipse ratio of 2.0) with diffuser length-to-diameter ratios $L_D/D_{DE}$ of 0.43 and 0.61, respectively. Data are shown at a free-stream velocity of 45 meters per second and incidence angles of $0^o$, $40^o$, and $50^o$. At $0^o$ incidence angle there is little difference between the aerodynamic performance of the two diffuser lengths. At an incidence angle of $40^o$, however, with cowl A (shorter diffuser) at a value of 81 percent design corrected weight flow an internal flow separation was encountered which extended forward to the inlet lip. The internal flow was attached at this same weight flow with cowl B. At $50^o$ incidence angle, lip separation is indicated in figure 25 for both cowls A and B although the recovery level for cowl B (longer diffuser) is consistently higher.

Shown in figure 26 is a comparison between the aerodynamic performance of cowls C and D having the same inlet lip shape (contraction ratio of 1.44/1.30 and ellipse ratio of 2.0/2.9) with diffuser length-to-diameter ratios of 0.61 and 0.92, respectively. At $0^o$ incidence angle, the pressure recovery is slightly higher with cowl C (shorter diffuser) than D. However, increasing incidence angle to $50^o$ has less of an effect on cowl D than C. In fact, at $50^o$ incidence angle, the pressure recovery is higher for cowl D (longer diffuser) than with cowl C.

The effect of diffuser design on inlet aeroacoustic performance is shown in figure 27 for cowls A and B. The data indicate that over all conditions of free-stream velocity and incidence angle, cowl B, with the longer diffuser, provides more acoustic suppression at a given value of total pressure recovery than cowl A. This lower level of performance encountered with cowl A is attributed to a combination of higher total pressure losses due to the higher rate of flow diffusion and a possible reduction in the internal attenuation of the noise due to the shorter length. The shorter length results in fewer internal noise reflections where acoustic energy can be dissipated.

The aeroacoustic performance comparison between cowls C and D is shown in figure 28. At static conditions (fig. 28(a)) both cowls provide relatively poor acoustic performance. As already discussed, this probably resulted because of the sharp upper lip on those two cowls. At 45 meters per second and an incidence angle of $0^o$ (fig. 28(b)) the aeroacoustic performance of the two cowls is about the same with perhaps slightly better performance of cowl D (longer diffuser) at the higher levels of suppression for the limited amount of data shown. At a $40^o$ incidence angle (fig. 28(c)) the longer diffuser of cowl D provides a greater amount of noise suppression at a given value of pressure recovery than cowl C.

Bulb-shaped centerbody approach geometry. - Figure 29 presents the aerodynamic results for the bulb-shaped centerbody approach geometry with cowls C and D. The effect of the longer diffuser of cowl D is to improve the high incidence angle performance

just as was the case for the cylindrical centerbody takeoff geometry (fig. 26). The aeroacoustic data presented in figure 30 indicate that statically and at a free-stream velocity of 45 meters per second at $0^{\circ}$ incidence angle (figs. 30(a) and (b)), the longer diffuser of cowl D may be providing slightly better performance. However, at $40^{\circ}$ incidence angle (fig. 30(c)), it is unclear, due to a limited amount of data, which diffuser is providing the best inlet acoustic performance.

In summary, the results presented in this discussion indicate that the primary effect of increasing sonic inlet diffuser length was to generally provide a greater amount of noise suppression at a given level of inlet pressure recovery. Changing diffuser length appeared to have little effect on inlet lip separation limits. However, a general trend toward higher recoveries at high incidence angles was detected when diffuser length was increased.

## SUMMARY OF RESULTS

A series of tests were conducted to determine the aerodynamic and acoustic performance of several sonic inlet takeoff and approach geometries. The takeoff geometries were (1) cylindrical centerbody and (2) bulb-shaped centerbody. The approach geometries were (1) bulb-shaped centerbody, (2) centerbody-annular ring, (3) annular ring, (4) radial vane, and (5) step diffuser. Effects of inlet lip and diffuser design were also investigated. The inlets were tested at static conditions and at a free-stream velocity of 45 meters per second at incidence angles from $0^{\circ}$ to $50^{\circ}$. The major results can be summarized as follows:

1. In terms of the highest inlet pressure recovery for a given amount of noise suppression, the cylindrical centerbody takeoff geometry and the bulb-shaped centerbody approach geometry provided the best results over the conditions of free-stream velocity and incidence angle tested. At a free-stream velocity of 45 meters per second and an incidence angle of $0^{\circ}$, the cylindrical centerbody takeoff geometry provided 20 decibels of noise suppression at the blade passing frequency with a total pressure recovery of 0.988 and a total pressure distortion of 0.008. At the same free-stream velocity and incidence angle, the bulb-shaped centerbody approach geometry provided 15 decibels of noise suppression with a recovery of 0.968 and a distortion of 0.130.

2. With the single passage geometries, increasing incidence angle (prior to lip separation) increased total pressure distortion as a result of a tendency for the total pressure losses to collect in the lower (windward) portion of the inlet. The only exception was the step diffuser approach geometry where the forced total pressure loss at the tip remained circumferentially uniform as the incidence angle was increased.

3. The two annular ring approach geometries did not provide the full amount of acoustic suppression measurable at static conditions, particularly at frequencies below

the blade passing. At some frequencies, these geometries actually produced more noise than the baseline inlet geometry.

4. With the radial vane approach geometry, the full amount of measurable noise suppression was obtained but the total pressure recovery was relatively low. The high losses encountered with this geometry were attributed to the drag rise characteristics of the vane airfoil sections and high vane solidity near the hub.

5. Increasing inlet cowl lower lip area contraction ratio from 1.30 to 1.44 resulted in a general improvement in inlet aerodynamic performance for the cylindrical centerbody takeoff geometry and bulb-shaped centerbody approach geometry as incidence angle was increased at a free-stream velocity of 45 meters per second. This increase in contraction ratio also increased the maximum incidence angle for attached flow from $40^{\circ}$ to at least $50^{\circ}$ for the cylindrical centerbody takeoff geometry. Increasing internal lip ellipse ratio from 2.0 to 2.9 apparently resulted in an increase in fan noise generation and a reduction in inlet noise suppression capability for the cylindrical centerbody takeoff geometry.

6. Changing diffuser length appeared to have little effect on inlet lip separation limits. However, increasing diffuser length resulted in an increase in noise suppression at a given value of total pressure recovery with the cylindrical centerbody takeoff geometry. The effect was also observed with the bulb-shaped centerbody approach geometry, but to a lesser degree.

Lewis Research Center,
National Aeronautics and Space Administration,
Cleveland, Ohio, October 6, 1975,
505-05.

## REFERENCES

1. Miller, Brent A.; and Abbott, John M.: Aerodynamic and Acoustic Performance of Two Choked-Flow Inlets Under Static Conditions. NASA TM X-2629, 1972.

2. Miller, Brent A.; and Abbott, John M.: Low-Speed Wind-Tunnel Investigation of the Aerodynamic and Acoustic Performance of a Translating-Centerbody Choked-Flow Inlet. NASA TM X-2773, 1973.

3. Abbott, John M.; Miller, Brent A.; and Golladay, Richard L.: Low-Speed Wind-Tunnel Investigation of the Aerodynamic and Acoustic Performance of a Translating-Grid Choked-Flow Inlet. NASA TM X-2966, 1974.

4. Chestnutt, David: Noise Reduction by Means of Inlet-Guide-Vane Choking in an Axial-Flow Compressor. NASA TN D-4682, 1968.

5. Klujber, F.; Bosch, J. C.; Demetrick, R. W.; and Robb, W. L.: Investigation of Noise Suppression by Sonic Inlets for Turbofan Engines. (D6-40855-Vol.-1, Boeing Commercial Airplane Co.; NAS3-15574.), NASA CR-121126, 1973.

6. Klujber, F.: Results of an Experimental Program for the Development of Sonic Inlets for Turbofan Engines. AIAA Paper 73-222, Jan. 1973.

7. Groth, Harold W.: Sonic Inlet Noise Attenuation and Performance with a J-85 Turbojet Engine as a Noise Source. AIAA Paper 74-91, Jan. 1974.

8. Albers, James A.: Predicted Upwash Angles at Engine Inlets for STOL Aircraft. NASA TM X-2593, 1972.

9. Yuska, Joseph A.; Diedrich, James H.; and Clough, Nestor: Lewis 9- by 15-Foot V/STOL Wind Tunnel. NASA TM X-2305, 1971.

10. Installation and Performance Data, Model TD-652, 5.5-Inch Tip Turbine Fan. Tech Development Inc., 1969.

11. Albers, James A.; and Miller, Brent A.: Effect of Subsonic Inlet Lip Geometry on Predicted Surface and Flow Mach Number Distributions. NASA TN D-7446, 1973.

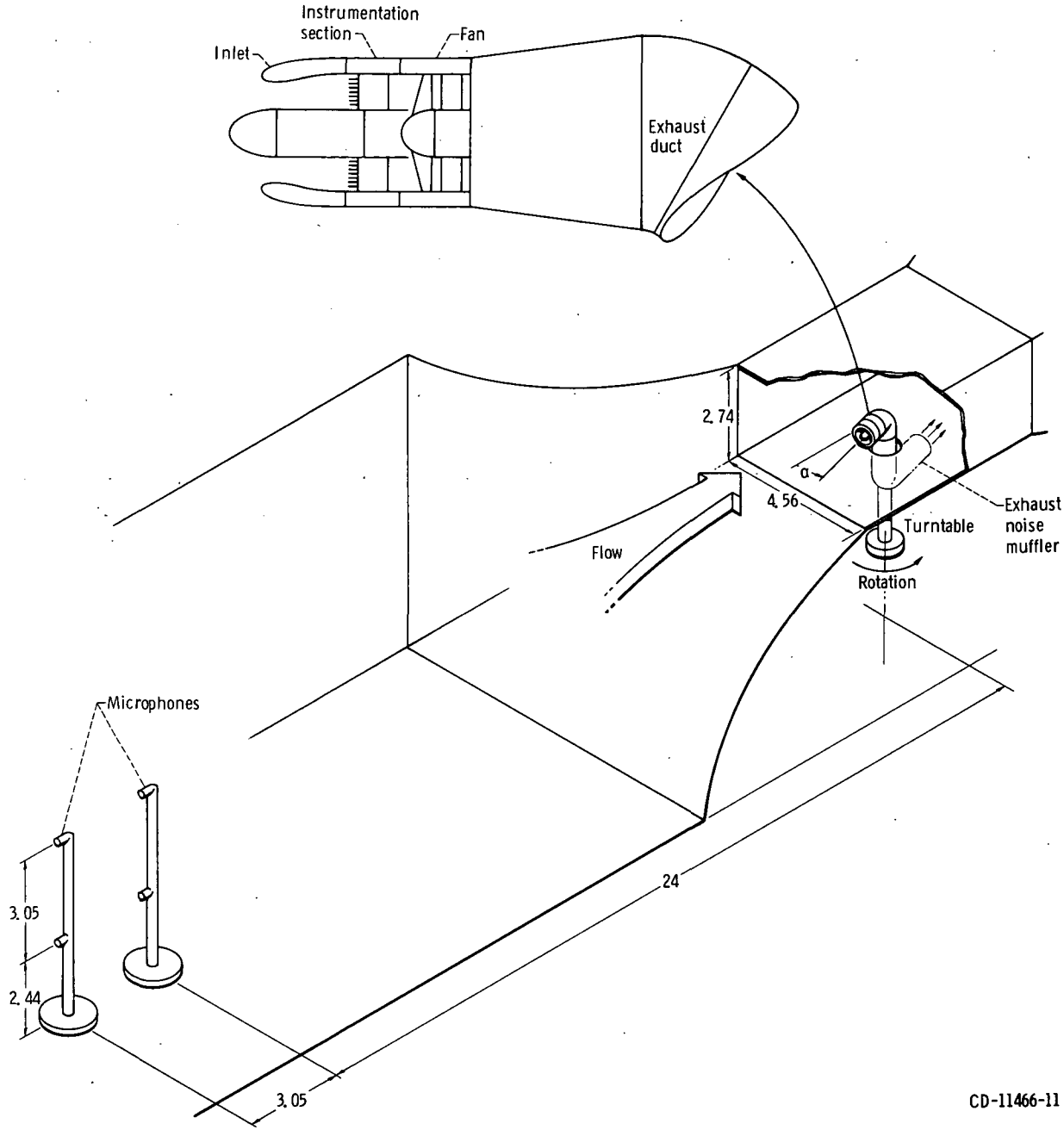


Figure 1. - Schematic view of V/STOL wind tunnel showing model and microphone locations. (All dimensions in m.)

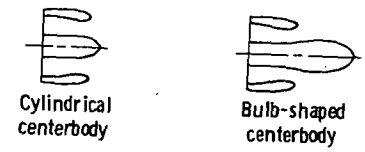


(a) Takeoff; $A_{DE}/A_{TH}$, 1.30.

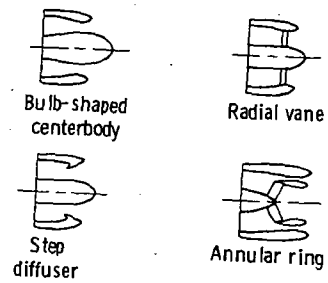


(b) Approach; $A_{DE}/A_{TH}$, 1.65.

(c) Baseline (cruise); $A_{DE}/A_{TH}$, 1.09.

Figure 2. - Inlet geometries tested.

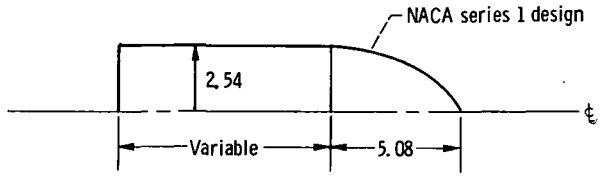


(a) Cylindrical centerbody.

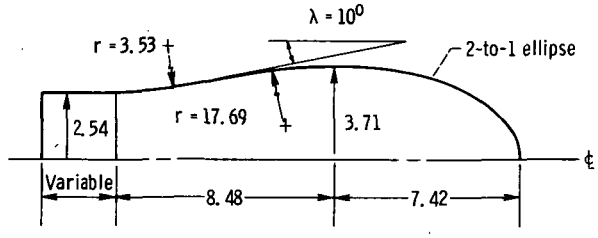


(b) Bulb-shaped centerbody.

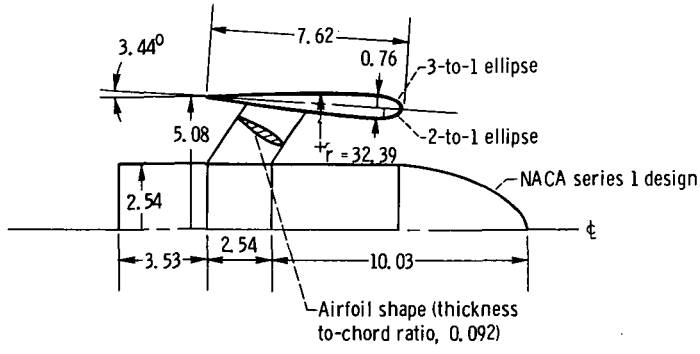


(c) Centerbody-annular ring.

Figure 3. - Inlet components utilized for throat area variation. (All dimensions in cm unless indicated otherwise.)

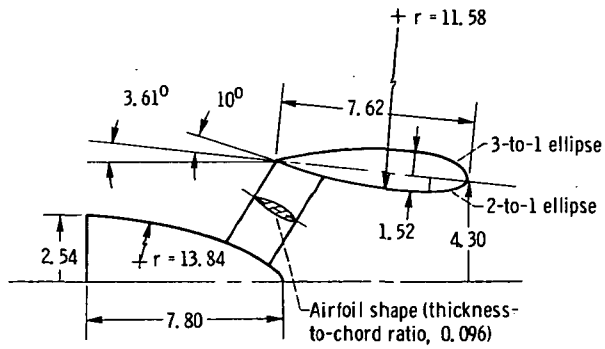


(d) Annular ring.

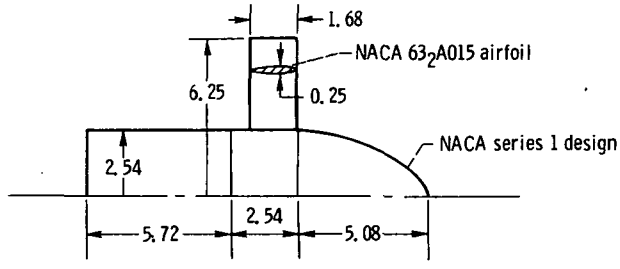


(e) Radial vane with cylindrical centerbody.

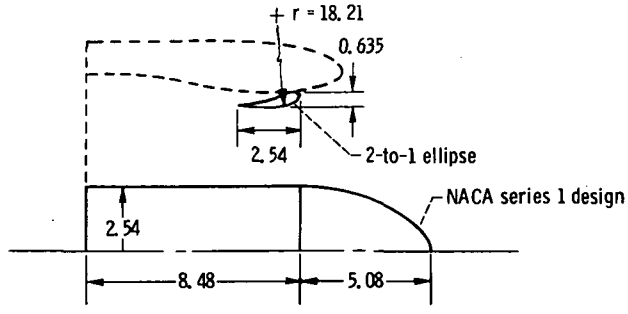


(f) Step diffuser with cylindrical centerbody.

Figure 3. - Concluded.

| Cowl | $(r_{HL}/r_{TH})^2$ | | a/b | | $r_{HL}/r_M$ | | $\frac{D_{DE}}{D_{TH}}$ | $\frac{L_D}{D_{DE}}$ | $\lambda_{max}$, deg |
|---|---|---|---|---|---|---|---|---|---|
| | $\psi = 0^0$ | $\psi = 180^0$ | $\psi = 0^0$ | $\psi = 180^0$ | $\psi = 0^0$ | $\psi = 180^0$ | | | |
| A | 1.30 | 1.30 | 2 | 2 | 0.87 | 0.87 | 1.12 | .43 | 13.6 |
| B | 1.30 | ↓ | ↓ | 2 | .87 | ↓ | ↓ | .61 | 9.3 |
| C | 1.44 | ↓ | ↓ | 2.9 | .91 | ↓ | ↓ | .61 | 9.3 |
| D | 1.44 | ↓ | ↓ | 2.9 | .91 | ↓ | ↓ | .92 | 3.2 |

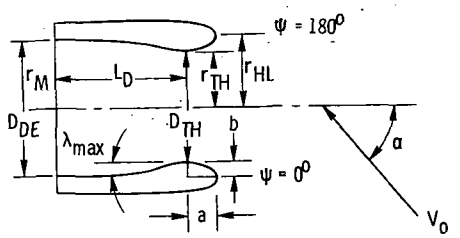


Figure 4. - Cowl geometries.

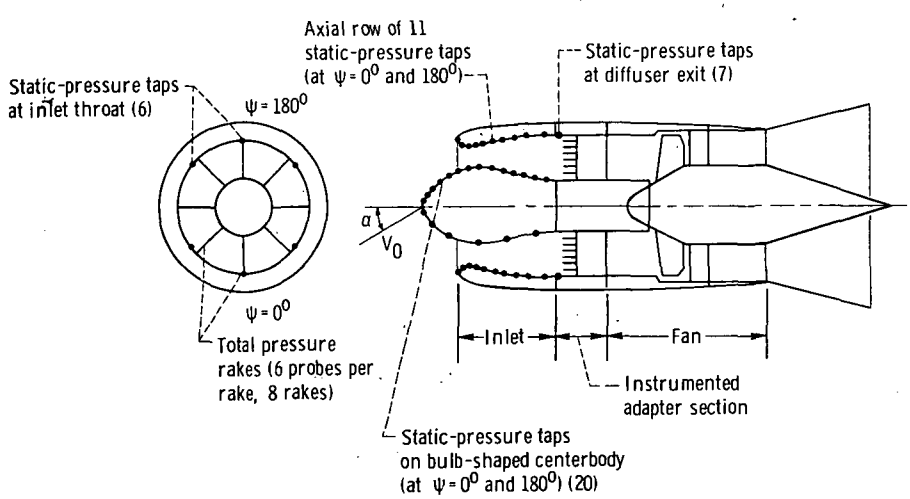


Figure 5. - Schematic view of test model showing location of instrumentation.

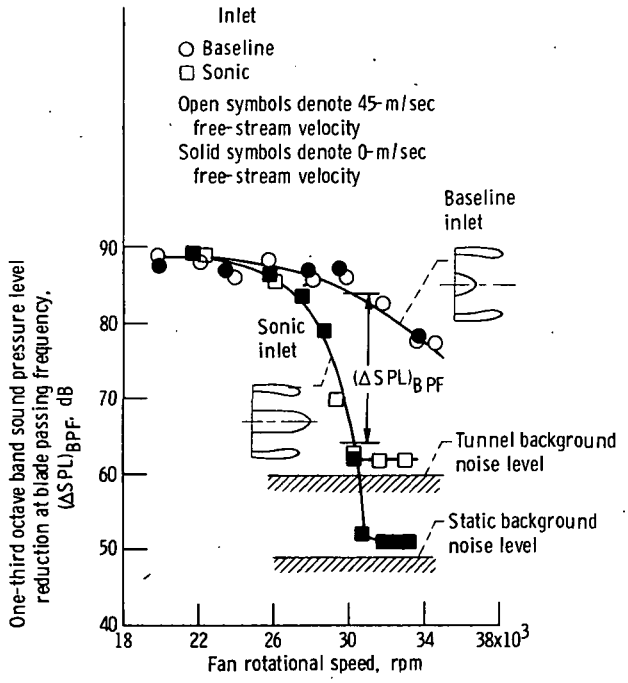


Figure 6. - Illustration of procedure used to determine noise suppression. Incidence angle, α, $0^0$.

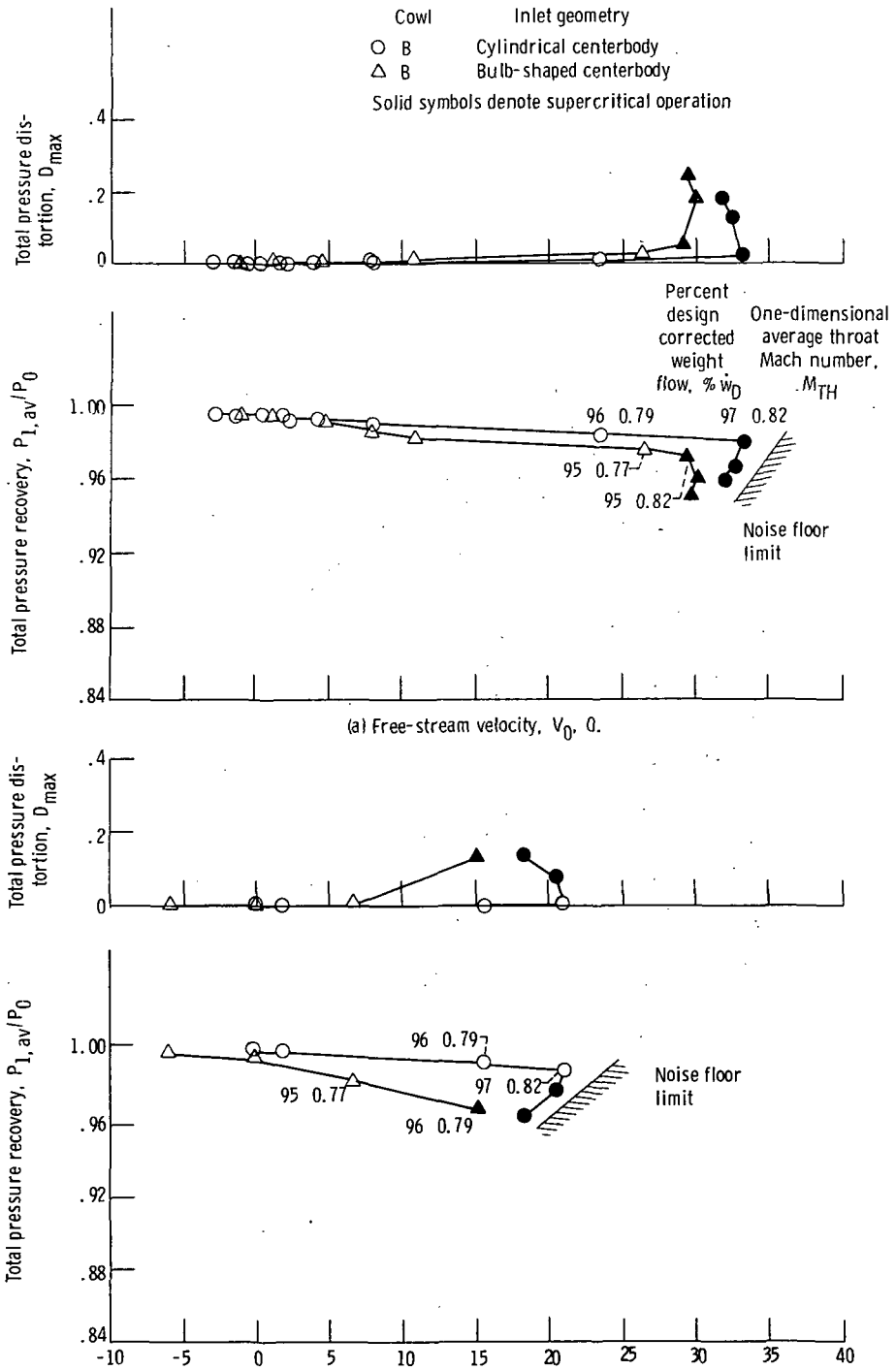


*Figure 7. - Aerodynamic and acoustic performance at sonic inlet takeoff geometries.*

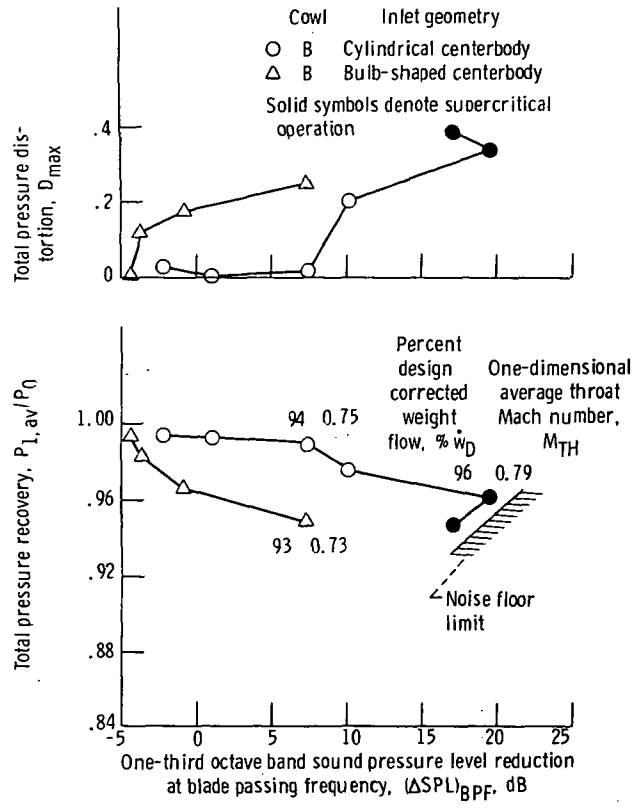


(c) Free-stream velocity, $V_0$, 45 meters per second; incidence angle, $\alpha$, 40°.

Figure 7. - Concluded.

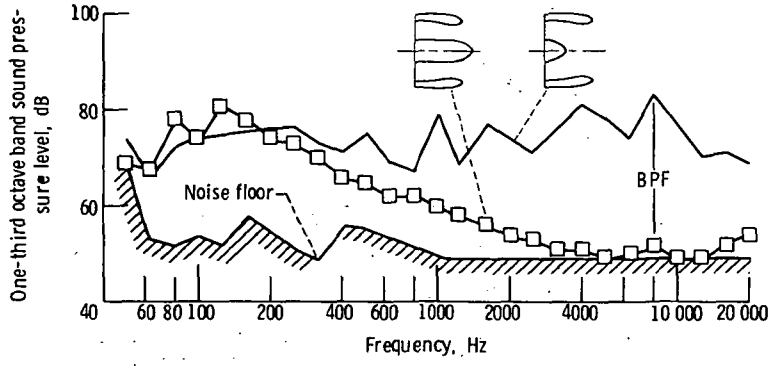


Figure 8. - Noise spectrum at maximum BPF suppression for cylindrical centerbody takeoff geometry. Cowl B; percent design corrected weight flow, % $\dot{w}_D$, 97; free-stream velocity, $V_0$, 0.

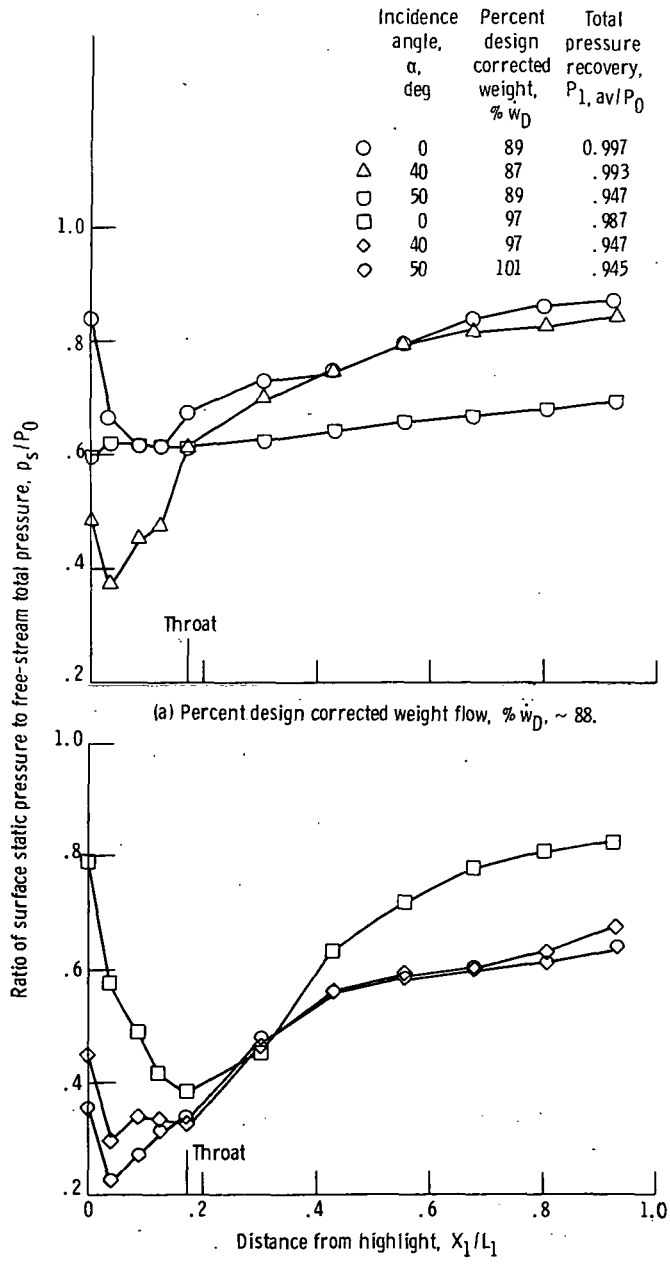


(a) Percent design corrected weight flow, % $w_D$, ~ 88.

(b) Percent design corrected weight flow, % $w_D$, ~ 97.

Figure 9. - Axial variation of cowl surface static pressure at $\psi = 0^0$ for cylindrical centerbody takeoff geometry. Cowl B; free-stream velocity, $V_0$, 45 meters per second.

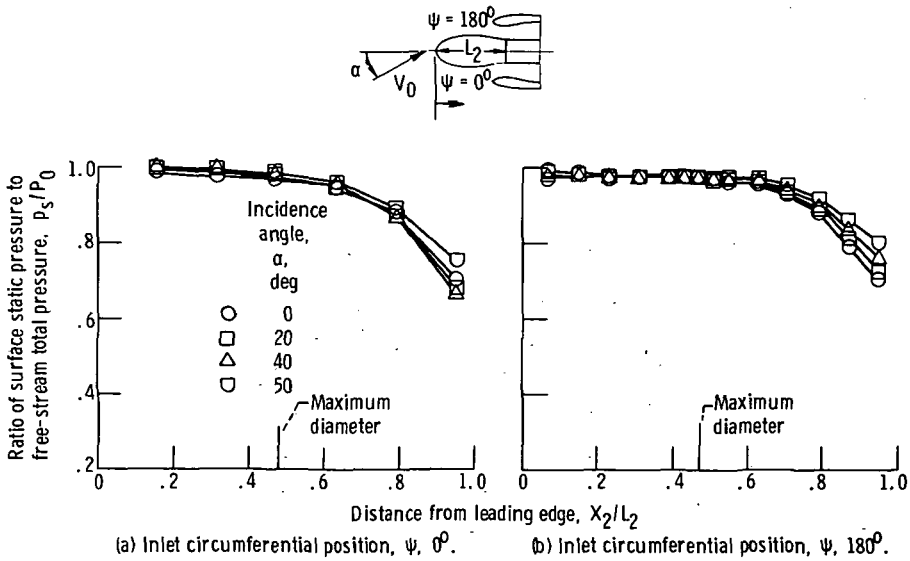


(a) Inlet circumferential position, ψ, 0°. (b) Inlet circumferential position, ψ, 180°.

Figure 10. - Axial variation of bulb-shaped centerbody surface static pressure for bulb-shaped centerbody takeoff geometry. Cowl B; percent design corrected weight flow, $\% \dot{w}_D$, ~95; free-stream velocity, $V_0$, 45 meters per second.

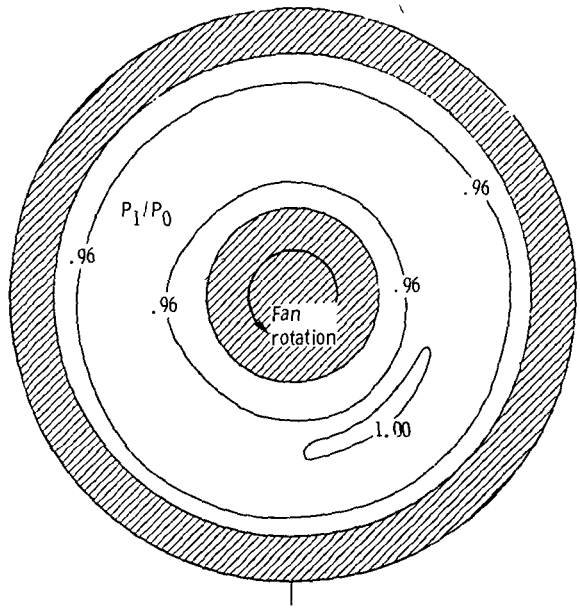


(a) Incidence angle, $\alpha$, $0^0$; percent design corrected weight flow, $\%\ \dot{w}_D$, 96; total pressure recovery, $P_{1,av}/P_0$, 0.966.

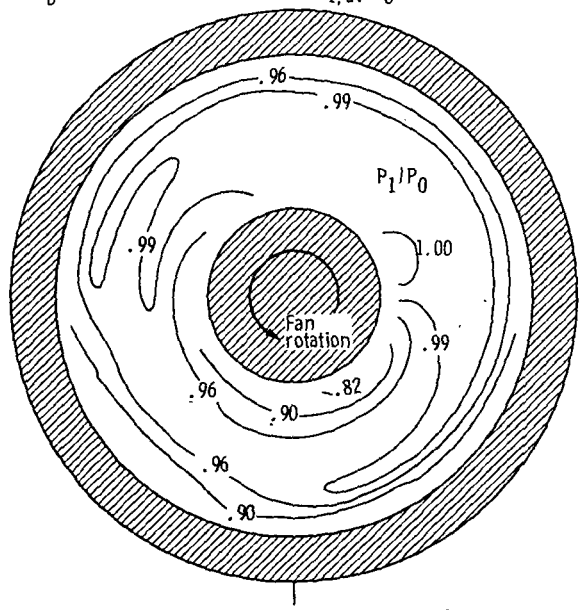


Inlet circumferential position, $\psi = 0^0$

(b) Incidence angle, $\alpha$, $20^0$; percent design corrected weight flow, $\%\ \dot{w}_D$, 98; total pressure recovery, $P_{1,av}/P_0$, 0.959.

Figure 11. - Total pressure distribution at diffuser exit for bulb-shaped centerbody, takeoff geometry. Cowl B; free-stream velocity, $V_0$, 45 meters per second.

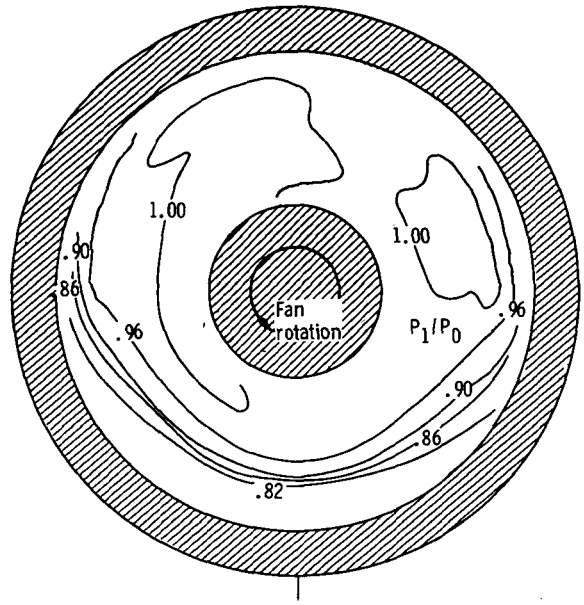


(c) Incidence angle, α, 40°; percent design corrected weight flow, % $\dot{w}_D$, 93; total pressure recovery, $P_{1,av}/P_0$, 0.949.

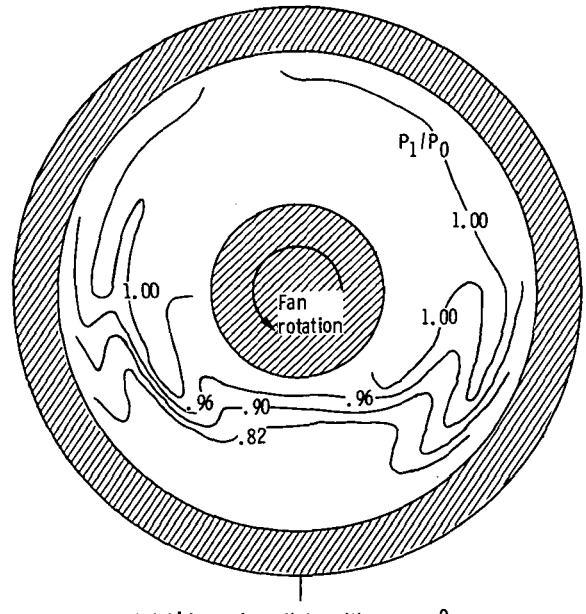


Inlet circumferential position, $\psi = 0^\circ$

(d) Incidence angle, α, 50°; percent design corrected weight flow, % $\dot{w}_D$, 93; total pressure recovery, $P_{1,av}/P_0$, 0.929.

Figure 11. - Concluded.

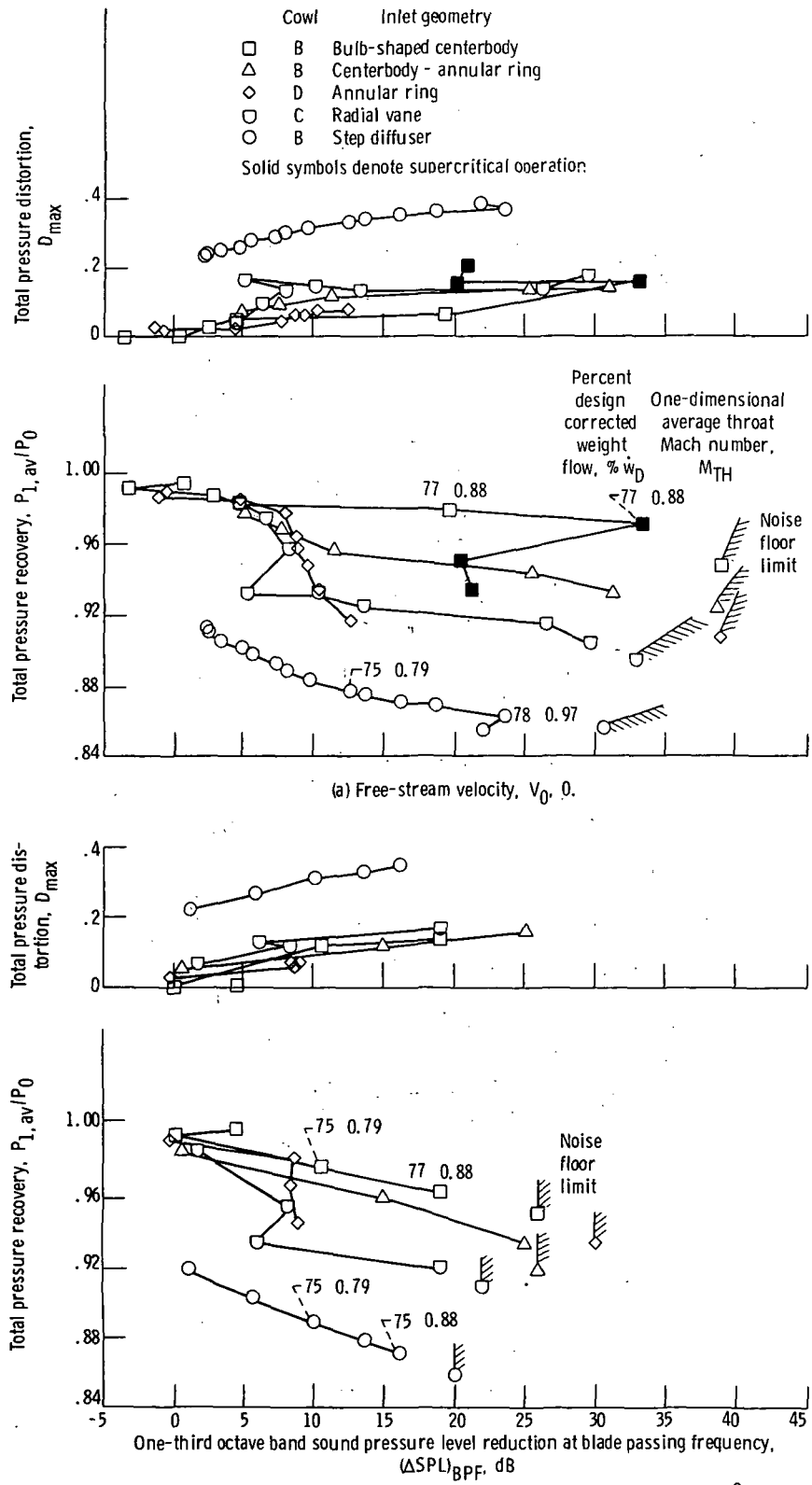


Figure 12. - Aerodynamic and acoustic performance of sonic inlet approach geometries.

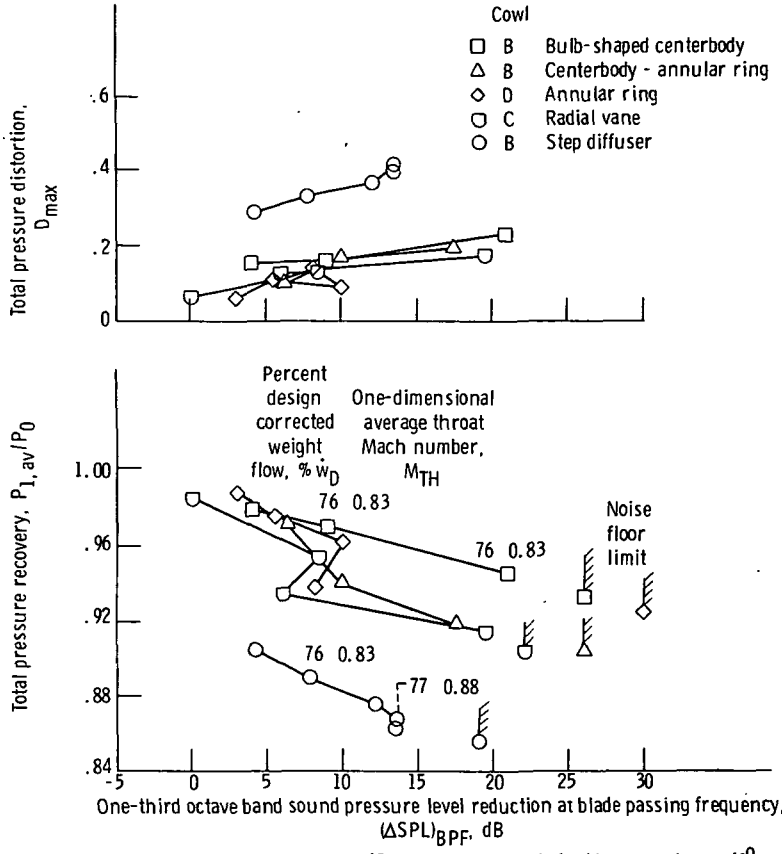


(c) Free-stream velocity, $V_0$, 45 meters per second; incidence angle, $\alpha$, $40^0$.

Figure 12. - Concluded.

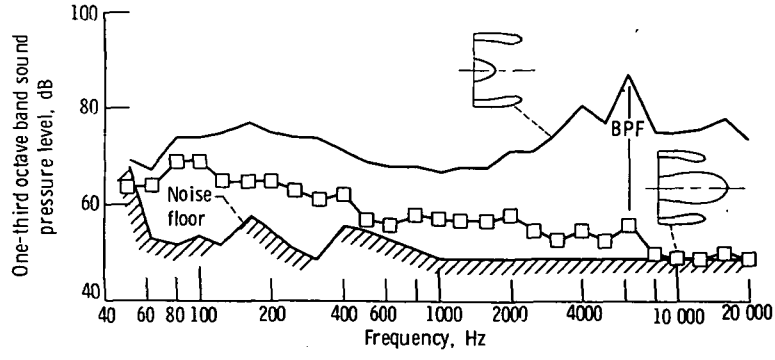


Figure 13. - Noise spectrum at maximum BPF suppression for bulb-shaped centerbody approach geometry. Cowl B; percent design corrected weight flow, $\% \dot{w}_D$, 77; free-stream velocity, $V_0$, 0.

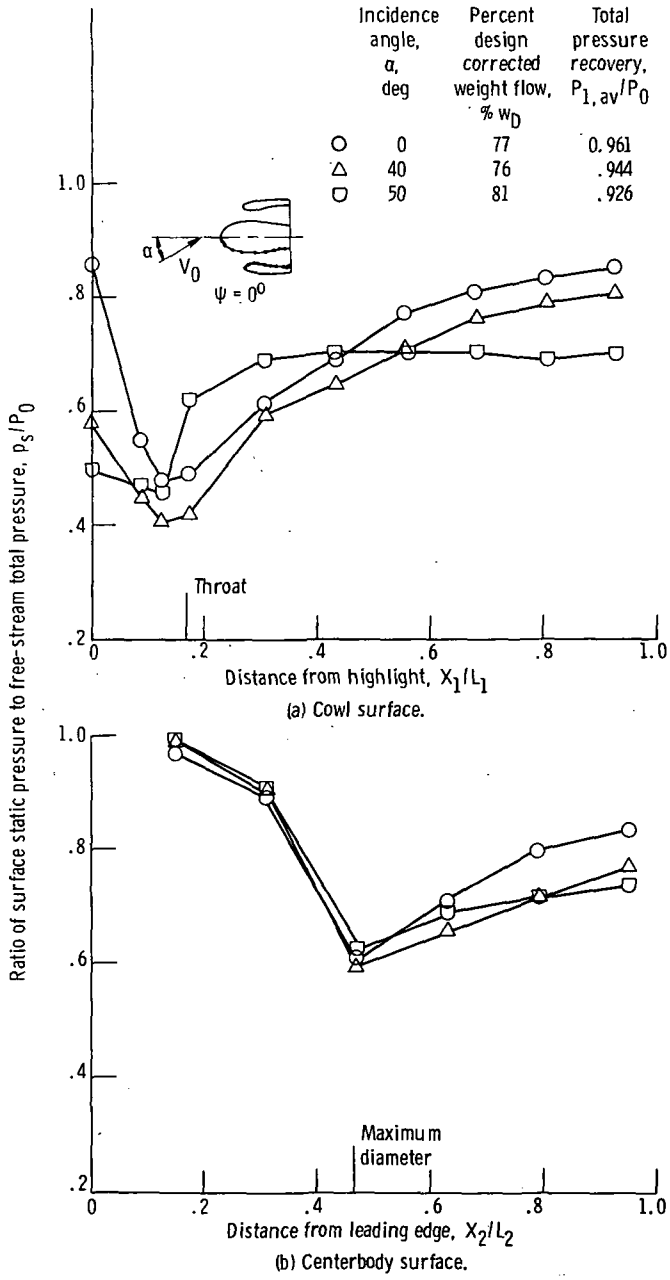


Figure 14. - Axial variation of surface static pressure at $\psi = 0^0$ for bulb-shaped centerbody approach geometry. Cowl B; free-stream velocity, $V_0$, 45 meters per second.

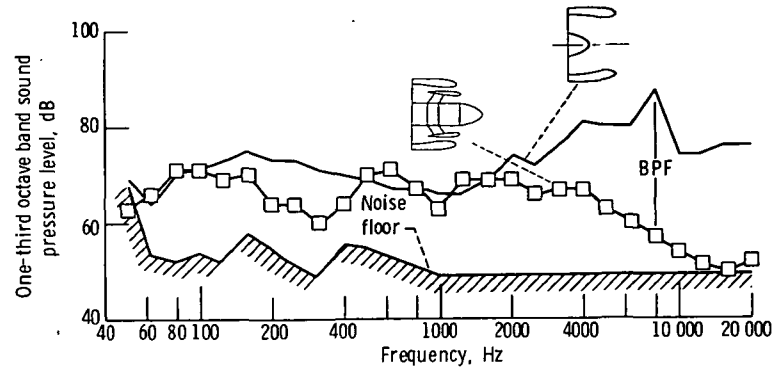


Figure 15. - Noise spectrum at maximum BPF suppression for centerbody annular ring approach geometry. Cowl B; one-third octave band sound pressure level reduction at blade passing frequency, $(\Delta SPL)_{BPF}$, 31 decibels; free-stream velocity, $V_0$, 0.

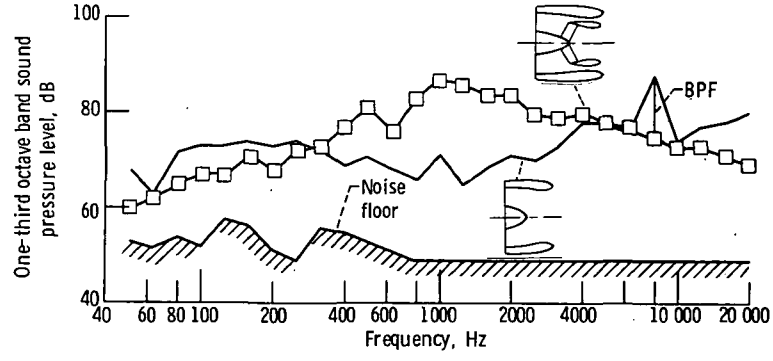


Figure 16. - Noise spectrum at maximum BPF suppression for annular ring approach geometry. Cowl D; one-third octave band sound pressure level reduction at blade passing frequency, $(\Delta SPL)_{BPF}$, 12.5 decibels; free-stream velocity, $V_0$, 0.

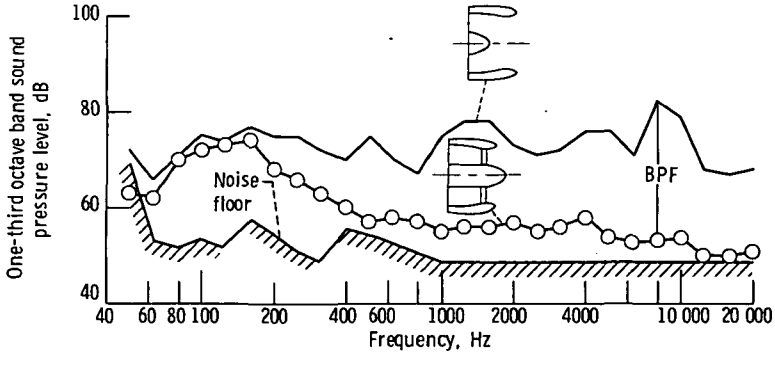


Figure 17. - Noise spectrum at maximum BPF suppression for radial vane approach geometry. Cowl C; one-third octave band sound pressure level reduction at blade passing frequency, $(\Delta SPL)_{BPF}$, 29 decibels; free-stream velocity, $V_0$, 0.

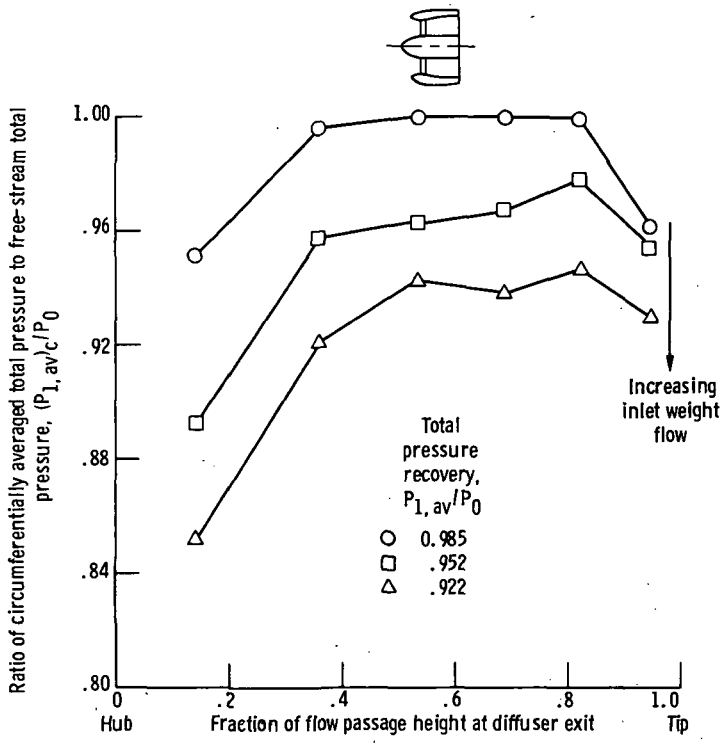


Figure 18. - Radial variation of total pressure at diffuser exit for radial vane approach geometry. Cowl C; free-stream velocity, $V_0$, 45 meters per second; incidence angle, $\alpha$, $0^0$.

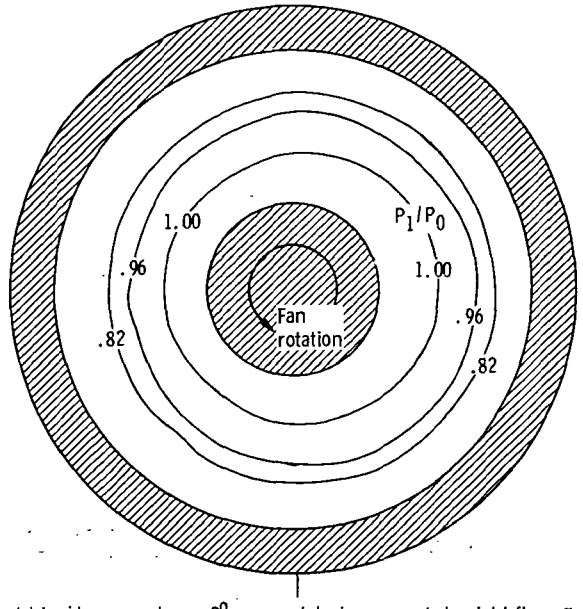


(a) Incidence angle, $\alpha$, $0^0$; percent design corrected weight flow, % $\dot{w}_D$, 76; total pressure recovery, $P_{1,av}/P_0$, 0.878.

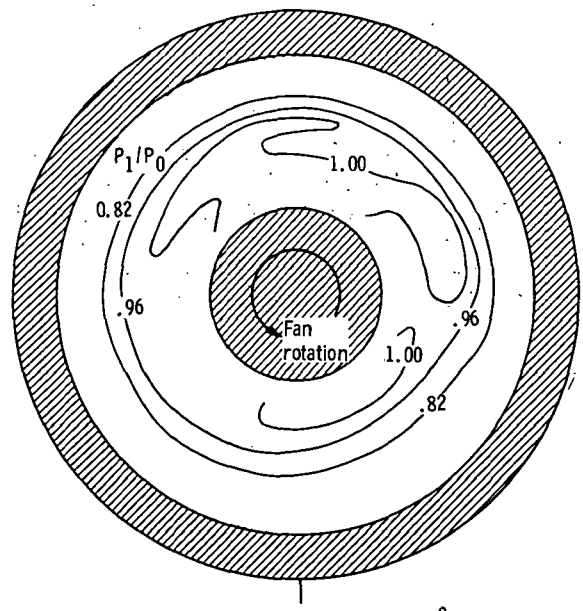


Inlet circumferential position, $\psi = 0^0$

(b) Incidence angle, $\alpha$, $50^0$; percent design corrected weight flow, % $\dot{w}_D$, 78; total pressure recovery, $P_{1,av}/P_0$, 0.866.

Figure 19. - Total pressure distribution at diffuser exit for step diffuser approach geometry. Cowl B; free-stream velocity, $V_0$, 45 meters per second.

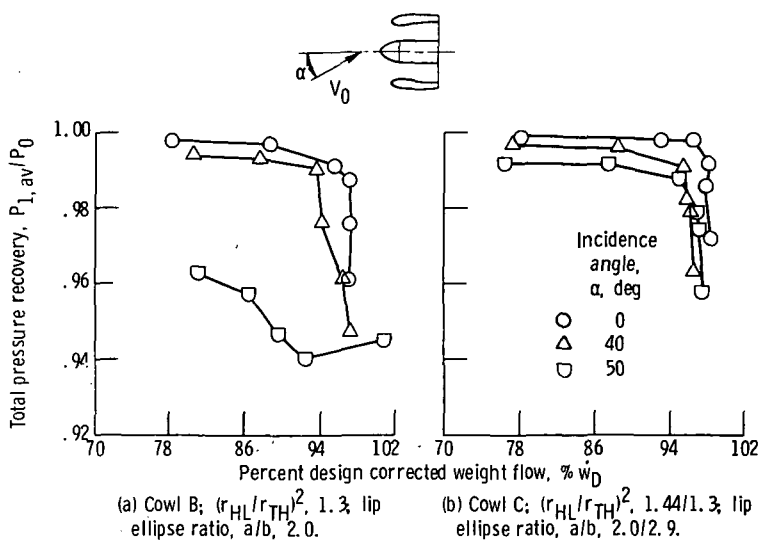


(a) Cowl B; $(r_{HL}/r_{TH})^2$, 1.3; lip ellipse ratio, a/b, 2.0.

(b) Cowl C; $(r_{HL}/r_{TH})^2$, 1.44/1.3; lip ellipse ratio, a/b, 2.0/2.9.

Figure 20. - Effect of lip design on aerodynamic performance of cylindrical centerbody takeoff geometry. Free-stream velocity, $V_0$, 45 meters per second.

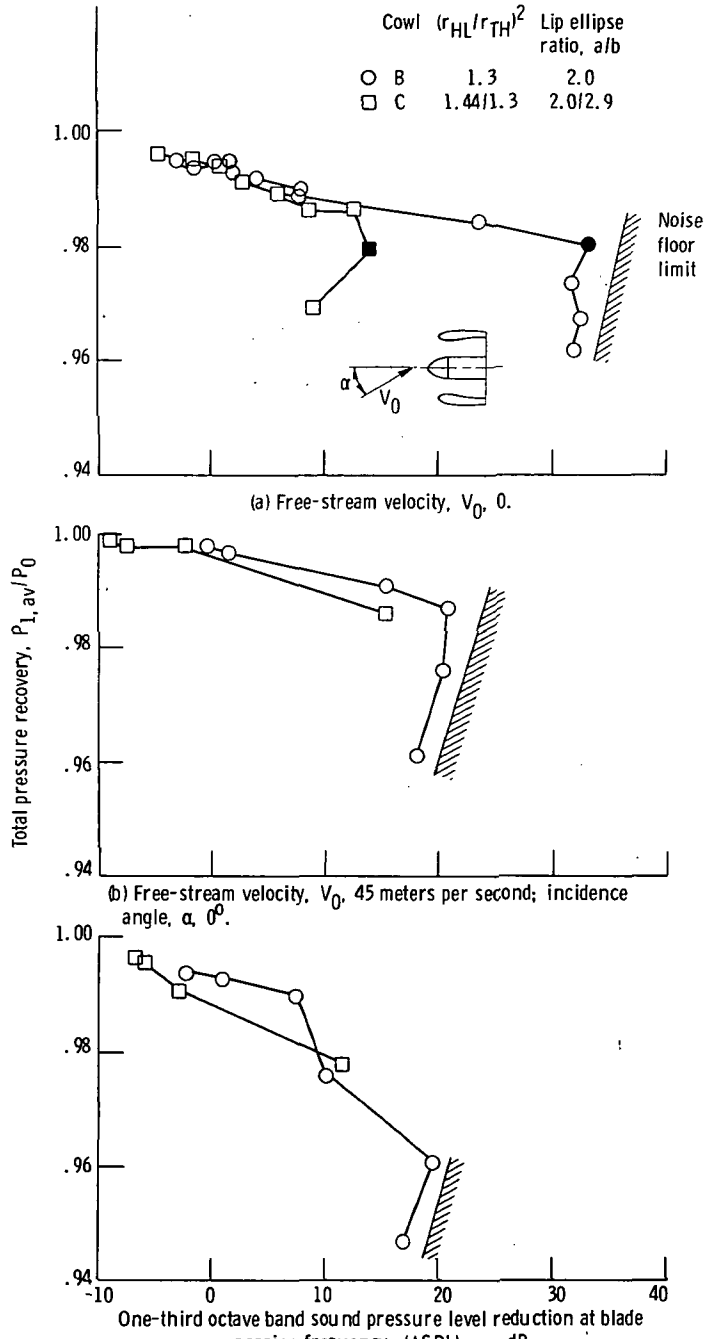


(a) Free-stream velocity, $V_0$, 0.

(b) Free-stream velocity, $V_0$, 45 meters per second; incidence angle, α, $0^0$.

(c) Free-stream velocity, $V_0$, 45 meters per second; incidence angle, α, $40^0$.

Figure 21. - Effect of lip design on aerodynamic and acoustic performance of cylindrical centerbody takeoff geometry.

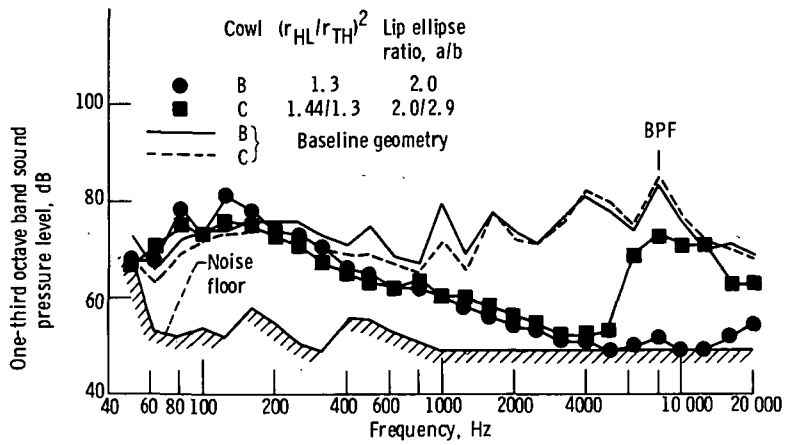


Figure 22. - Effect of lip design on noise spectra for cylindrical centerbody take-off geometry. Free-stream velocity, $V_0$, 0.

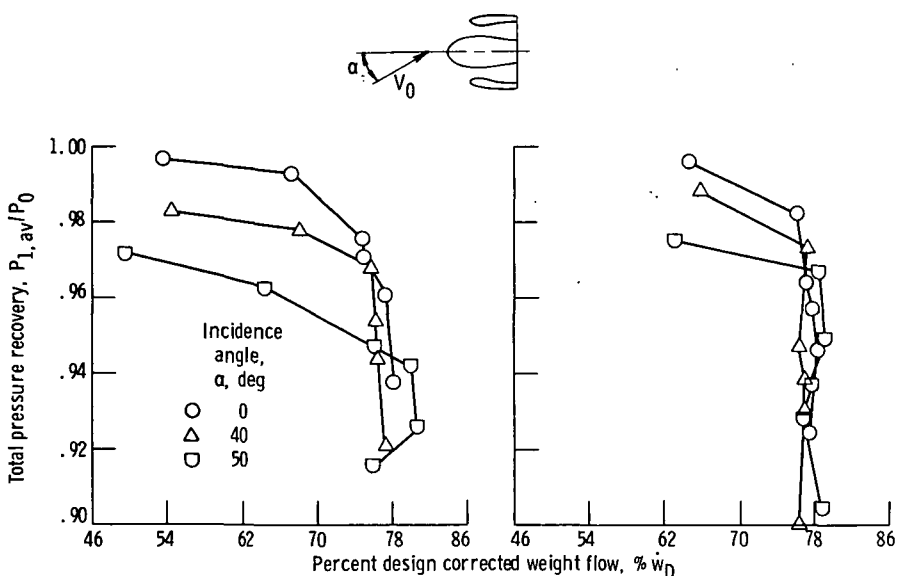


(a) Cowl B; $(r_{HL}/r_{TH})^2$, 1.3; lip ellipse ratio a/b, 2.0.

(b) Cowl C; $(r_{HL}/r_{TH})^2$, 1.44/1.3; lip ellipse ratio, a/b. 2.0/2.9.

Figure 23. - Effect of lip design on aerodynamic performance of bulb-shaped centerbody approach geometry. Free-stream velocity, $V_0$, 45 meters per second.

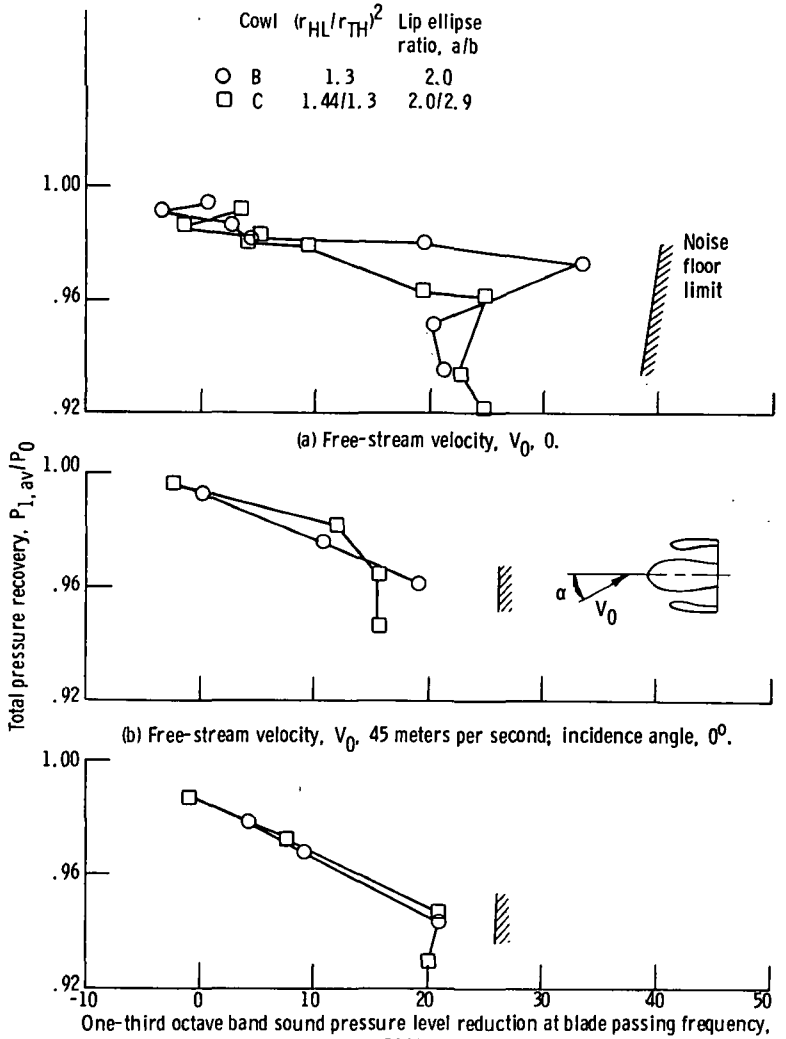


Figure 24. - Effect of lip design on aerodynamic and acoustic performance of bulb-shaped centerbody approach geometry.

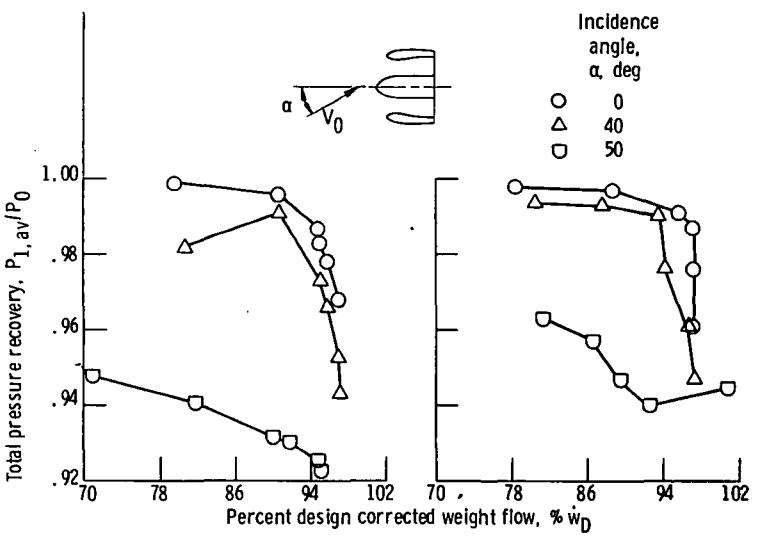


Figure 25. - Effect of diffuser design on aerodynamic performance of cylindrical centerbody takeoff geometry. Free-stream velocity, $V_0$, 45 meters per second; $(r_{HL}/r_{TH})^2$, 1.3; lip ellipse ratio, a/b, 2.0.

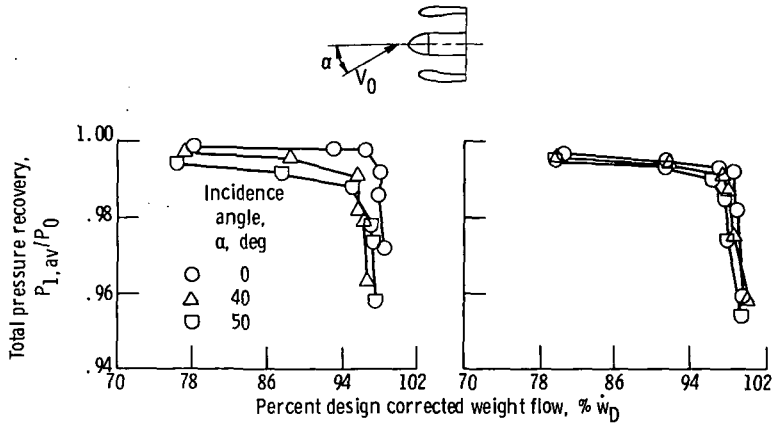


(a) Cowl C; length-to-diameter ratio, $L_D/D_{DE}$, 0.61.

(b) Cowl D; length-to-diameter ratio, $L_D/D_{DE}$, 0.92.

Figure 26. - Effect of diffuser design on aerodynamic performance of cylindrical centerbody takeoff geometry. Free-stream velocity, $V_0$, 45 meters per second; $(r_{HL}/r_{TH})^2$, 1.44/1.3; lip ellipse ratio, a/b, 2.0/2.9.

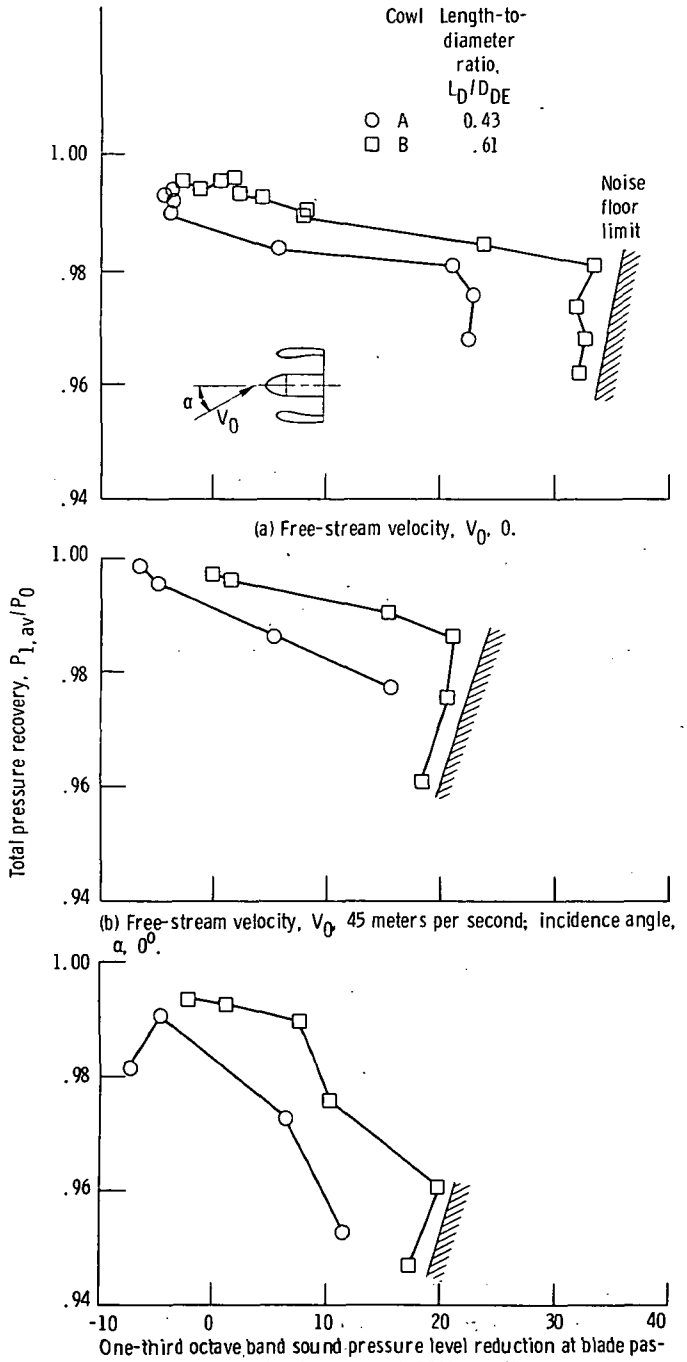


(a) Free-stream velocity, $V_0$, 0.

(b) Free-stream velocity, $V_0$, 45 meters per second; incidence angle, α, $0^0$.

(c) Free-stream velocity, $V_0$, 45 meters per second; incidence angle, α, $40^0$.

Figure 27. - Effect of diffuser design on aerodynamic and acoustic performance of cylindrical centerbody takeoff geometry. $(r_{HL}/r_{TH})^2$, 1.3; lip ellipse ratio, a/b, 2.0.

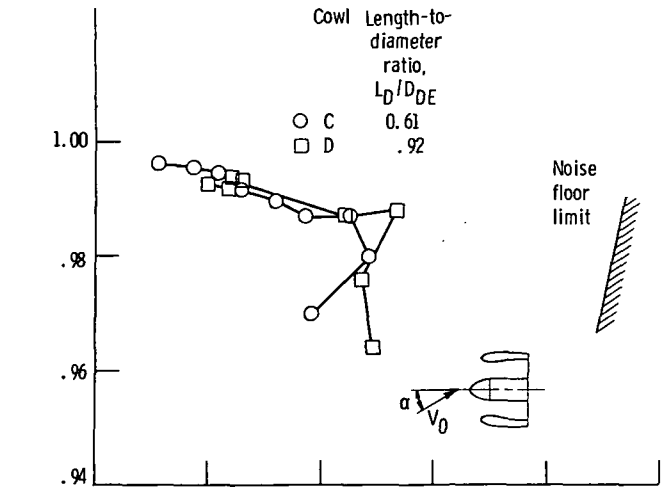


(a) Free-stream velocity, $V_0$, 0.

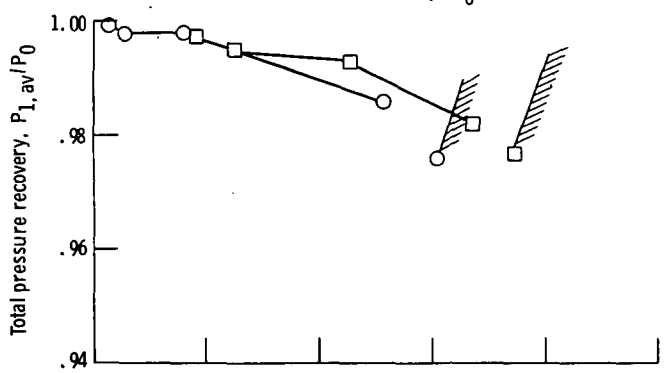


(b) Free-stream velocity, $V_0$, 45 meters per second; incidence angle, α, 0°.

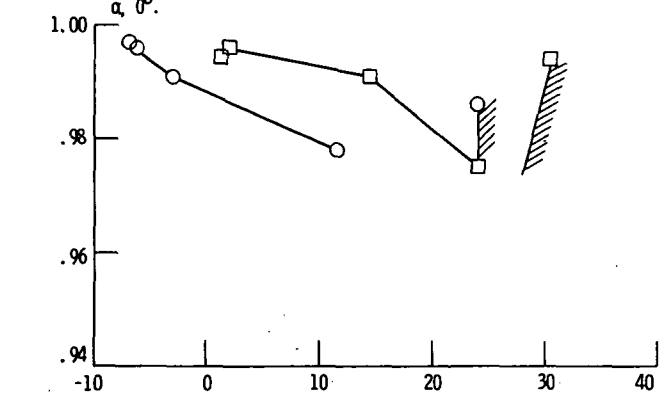


(c) Free-stream velocity, $V_0$, 45 meters per second; incidence angle, α, 40°.

Figure 28. - Effect of diffuser design on aerodynamic and acoustic performance of cylindrical centerbody takeoff geometry. $(r_{HL}/r_{TH})^2$, 1.44/1.3; lip ellipse ratio, a/b, 2.0/2.9.

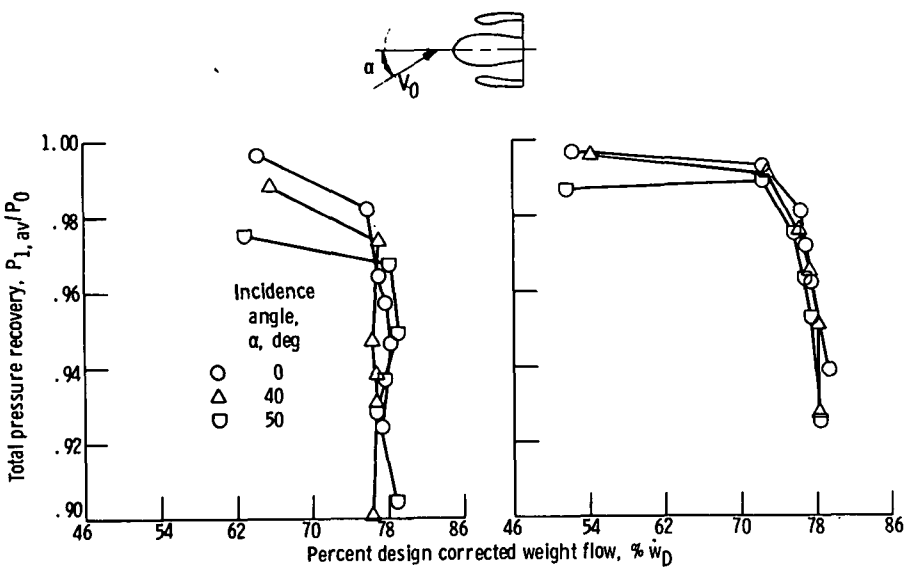


(a) Cowl C; length-to-diameter ratio, $L_D/D_{DE}$, 0.61.

(b) Cowl D; length-to-diameter ratio, $L_D/D_{DE}$, 0.92.

Figure 29. - Effect of diffuser design on aerodynamic performance of bulb-shaped centerbody approach geometry. Free-stream velocity, $V_0$, 45 meters per second; $(r_{HL}/r_{TH})^2$, 1.44/1.3; lip ellipse ratio, a/b, 2.0/2.9.

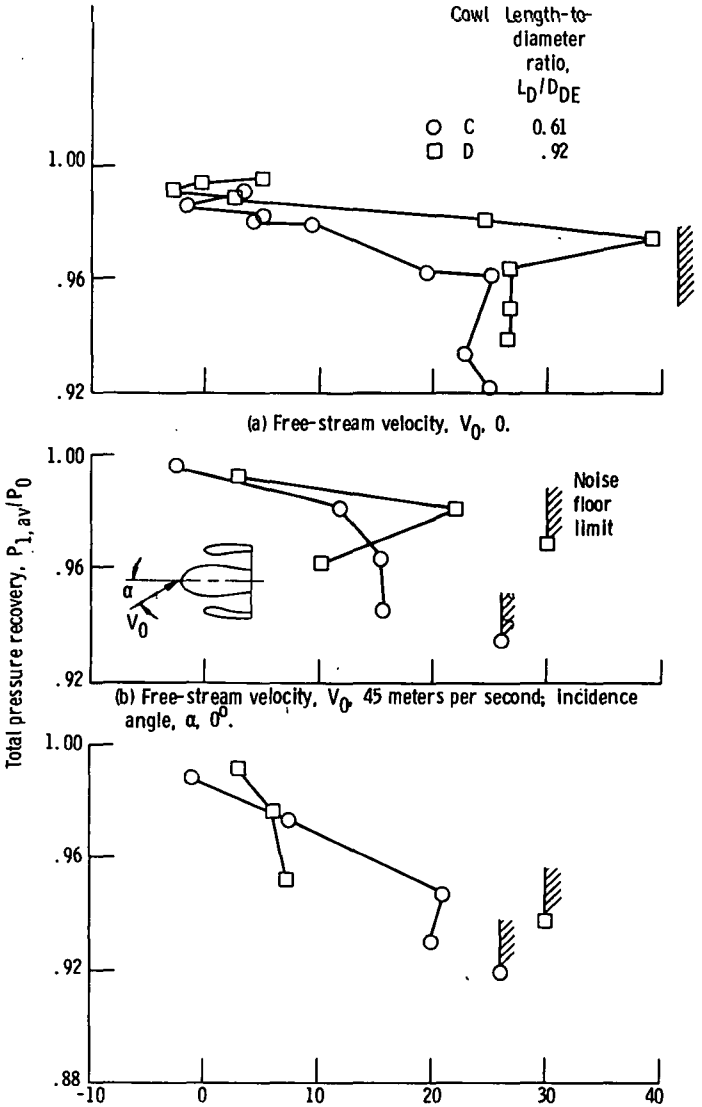


(a) Free-stream velocity, $V_0$, 0.

(b) Free-stream velocity, $V_0$, 45 meters per second; incidence angle, α, 0°.

(c) Free-stream velocity, $V_0$, 45 meters per second; incidence angle, α, 40°.

Figure 30. - Effect of diffuser design on aerodynamic and acoustic performance of bulb-shaped centerbody approach geometry. $(r_{HL}/r_{TH})^2$, 1.44/1.3; lip ellipse ratio, a/b, 2.0/2.9.

NATIONAL AERONAUTICS AND SPACE ADMINISTRATION
WASHINGTON, D.C. 20546

OFFICIAL BUSINESS
PENALTY FOR PRIVATE USE $300

SPECIAL FOURTH-CLASS RATE
BOOK

POSTAGE AND FEES PAID
NATIONAL AERONAUTICS AND
SPACE ADMINISTRATION
451

U.S.MAIL

POSTMASTER: If Undeliverable (Section 158 Postal Manual) Do Not Return

*"The aeronautical and space activities of the United States shall be conducted so as to contribute . . . to the expansion of human knowledge of phenomena in the atmosphere and space. The Administration shall provide for the widest practicable and appropriate dissemination of information concerning its activities and the results thereof."*

—NATIONAL AERONAUTICS AND SPACE ACT OF 1958

# NASA SCIENTIFIC AND TECHNICAL PUBLICATIONS

TECHNICAL REPORTS: Scientific and technical information considered important, complete, and a lasting contribution to existing knowledge.

TECHNICAL NOTES: Information less broad in scope but nevertheless of importance as a contribution to existing knowledge.

TECHNICAL MEMORANDUMS: Information receiving limited distribution because of preliminary data, security classification, or other reasons. Also includes conference proceedings with either limited or unlimited distribution.

CONTRACTOR REPORTS: Scientific and technical information generated under a NASA contract or grant and considered an important contribution to existing knowledge.

TECHNICAL TRANSLATIONS: Information published in a foreign language considered to merit NASA distribution in English.

SPECIAL PUBLICATIONS: Information derived from or of value to NASA activities. Publications include final reports of major projects, monographs, data compilations, handbooks, sourcebooks, and special bibliographies.

TECHNOLOGY UTILIZATION PUBLICATIONS: Information on technology used by NASA that may be of particular interest in commercial and other non-aerospace applications. Publications include Tech Briefs, Technology Utilization Reports and Technology Surveys.

***Details on the availability of these publications may be obtained from:***

**SCIENTIFIC AND TECHNICAL INFORMATION OFFICE**

**NATIONAL AERONAUTICS AND SPACE ADMINISTRATION**

**Washington, D.C. 20546**